Title: End-binding protein 1 controls signal propagation from the T Cell Receptor.

Authors: Martín-Cófreces Noa Beatriz [1,2], Baixauli Francesc [1,2], López María José[1,2], Gil Diana [3], Monjas Alicia [4], Alarcón Balbino [4] and Sánchez-Madrid Francisco [1,2,*].

Affiliation:

[1] Servicio de Inmunología, Hospital Universitario de la Princesa, Universidad Autónoma de Madrid, Instituto Investigación Sanitaria Princesa (IIS-IP), Madrid, 28006, Spain.

[2] Departamento de Biología Vascular e Inflamación, Centro Nacional de Investigaciones Cardiovasculares (CNIC), Madrid, 28029, Spain.

[3] Department of Immunology, College of Medicine, Mayo Clinic. Rochester, MN 55905, US.

[4] Centro de Biología Molecular Severo Ochoa (CBMSO), Madrid, 28049 Spain.

* Corresponding author.

Contact information:

Francisco Sánchez-Madrid
Laboratorio de Comunicación Intercelular
Servicio de Inmunología
Instituto de Investigación Sanitaria Princesa
Planta 1
Hospital de La Princesa
Diego de León 62
28006 Madrid
Spain
fsanchez.hlpr@salud.madrid.org
Phone: +34915202307
FAX: +34915202374

Character count: 48,324

Running Title: EB1 regulates TCR signaling.

Abstract

The role of microtubules in the control and dynamics of the IS remains unresolved. Here we show that T cell activation requires the growth of microtubules mediated by the plus-end specific protein end-binding 1 (EB1). A direct interaction of the T Cell Receptor (TCR) complex with EB1 provides the molecular basis for EB1 activity promoting TCR encounter with signaling vesicles at the IS. EB1 knockdown alters TCR dynamics at the IS and prevents propagation of the TCR activation signal to LAT, thus inhibiting activation of PLCγ1 and its localization to the IS. These results identify a role for EB1 interaction with the TCR in controlling TCR sorting and its connection with the LAT/PLCγ1 signalosome.

Keywords: T cell activation, cell signaling, vesicular trafficking, cytoskeleton, microtubule dynamics.

Introduction

The TCR complex is exposed on the surface of T cells, and is formed by heterodimers of ligand-binding subunits, either TCR-α and TCR-β (in αβ T cells) or TCR-γ and TCR-δ (in γδ T cells), which associate with the signal-transducing subunits CD3γ, -δ, -ε and -ζ (van der Merwe & Dushek, 2011). The cytoplasmic tails of CD3γ, -δ, and -ε contain a single copy of a motif called ITAM (immune-receptor tyrosine-based activation motif), whereas CD3ζ contains three ITAMs. ITAMs are phosphorylated upon TCR stimulation by kinases of the src family. Phosphorylated ITAMs are docking sites for SH2-domain containing proteins (Schamel et al, 2006). ITAM phosphorylation is necessary for the polarization of the centrosome to the immune synapse (IS) (Lowin-Kropf et al, 1998), which is therefore dependent on Lck and Fyn tyrosine kinase activity (Etienne-Manneville, 2010; Lowin-Kropf et al, 1998; Martin-Cofreces et al, 2006). Centrosome movement is dependent on the dynein/dynactin motor, which allows sustained TCR activation (Martin-Cofreces et al, 2008) and polarized secretion (Huse et al, 2008). The movement of the centrosome carries cytoplasmic organelles, including the Golgi, multivesicular bodies and the mitochondria network, toward the IS (Calabia-Linares et al, 2011), contributing to TCR signaling and IS formation (Baixauli et al, 2011).

The specific function of microtubules (MTs) in T cell activation is poorly understood. MTs are large polymers of α/β-tubulin dimers that control intracellular organelle distribution and trafficking (Etienne-Manneville, 2010). MTs show intrinsic polarity, with minus-ends that can anchor to the centrosome to avoid rapid de-polymerization (Li & Gundersen, 2008). MT plus-ends show dynamic instability, being able to switch between growing and shrinkage phases. End-binding proteins (EBs) are highly conserved and ubiquitous plus-end tracking proteins (+TIP)

(Tirnauer & Bierer, 2000). The three EBs (EB1, 2 and 3) are small dimeric proteins that contain an N-terminal calponin homology domain (CH) which is able to bind to MTs. These proteins possess, at their C-terminus, a flexible acidic tail that contains the sequence EEY/F, required for self-inhibition and binding to various partners, that can control microtubule growth (Akhmanova & Steinmetz, 2008; Manna et al, 2008).

In this study, EB1 was found to bind to the CD3 ITAMs. Knockdown of EB1 in T cells prevents TCR clustering at the IS and the correct phosphorylation of LAT and PLCγ1. We found that EB1 regulates vesicular trafficking at the IS and therefore the connection between the TCR and downstream signaling molecules, such as LAT/PLCγ1. These results suggest that TCR-EB1 interaction may play a dual role at the IS, controlling both TCR sorting and its encounter with the LAT/PLCγ1 signalosome.

Results

EB1 directly interacts with the CD3 ITAMs through its four-helix bundle.

To identify new interacting partners of the TCR complex, we used a yeast two-hybrid SOS-recruitment system to screen for CD3ε cytoplasmic tail-binding proteins. EB1 was identified in this screening (Supplementary Table S1). The isolated cDNA encodes the C-terminal third of EB1 (82 aminoacids). To confirm EB1-CD3ε interaction, we performed pull-down assays with GST-EB1 fusion protein in COS cells transfected with different CD3 subunits. CD3ε and CD3ζ, were recovered but not CD3γ or CD3δ (Figure 1A). GST-EB1 also co-precipitated a purified cytoplasmic fragment of CD3ζ (Supplementary Figure S1A), thus suggesting that EB1 interaction with CD3 subunits is direct.

ITAMs are the shared regions in the cytoplasmic tails of CD3ε and CD3ζ. Therefore, we assessed whether EB1 interacts with CD3ε and CD3ζ ITAMs using chimeric fusion proteins of CD8α with each of the three CD3ζ ITAMs (ζA, ζB and ζC), or the cytoplasmic tail of CD3ε. EB1 strongly co-precipitated with each of the three ITAMs from CD3ζ (CD8-ζC, CD8-ζA and CD8-ζB) as well as with CD8-ε, but not with CD8γ (Figure 1B). Therefore, the specificity for the ITAMS of CD3ζ and ε can be explained by the sequence of these ITAMs, which are less acidic than the ITAMs of CD3γ and δ (Figure 1B).

To characterize the CD3-binding site in EB1, we generated a panel of GST fusion proteins (Figure 1C). As predicted from the two-hybrid screen, CD3 bound to a construct, GST-Ct, which contained the C-terminal 82 amino acids of EB1. The first half of the α1 helix is not required for CD3 binding, since deletion of the first 10 or 20 amino acids (a and b constructs) did not prevent the EB1-CD3 interaction. Likewise, the acidic tail seems to be unnecessary since deletions d and e did not affect

the interaction. However, CD3-EB1 interaction was abrogated by simultaneous elimination of the acidic tail and half of the α1 helix (deletion be) or by either complete deletion of helix α2 or most of helix α1 (deletions f and c). These findings indicate that CD3 binds to the four-helix bundle of EB1.

To analyze whether the CD3-EB1 interaction takes place in T cells, EB1 was immunoprecipitated from murine thymocytes and spleen T cell lysates. EB1 was found associated to CD3ζ in cells from both organs (Supplementary Figure S1B). To study whether TCR stimulation affects CD3ζ interaction with EB1, anti-CD3 stimulated thymocytes and spleen T cells were immunoprecipitated with anti-CD3ζ. EB1 co-immunoprecipitated with the TCR in both cell lysates, independently of CD3 stimulation (Figure S1C). When EB1 immunoprecipitations were carried out with surface-biotinylated Jurkat T cells, two major biotinylated bands were detected, corresponding to the CD3ζ homodimer and the TCRα/β heterodimer, together with weak signals for CD3γ, CD3δ and CD3ε (Figure 1D). This result points to an EB1 association to a partial TCR complex that contains TCRαβ and CD3ζ. The effect may be due to a multichain immune receptor oligo-oligomerization, where the TCR and CD3 subunits dissociate upon stimulation (Sigalov, 2006). Alternatively, it could be due to a different rate of degradation for the TCR expressed on the surface, as TCRαβ degrades faster than CD3 chains in non-stimulated cells (San Jose & Alarcon, 1999). Since the association of EB1 with TCRαβ and CD3ζ is detected in non-stimulated T cells (Fig. 1D), this interaction may be involved in the trafficking of the most rapidly-degraded TCR subunits from the plasma membrane.

To further analyze whether EB1 binding to CD3ζ was altered by stimulation, CD3ζ was immunoprecipitated from primary CD8+ OT-I transgenic T cells stimulated by OVA antigen-loaded T2kb cells. The recovery of EB1 was similar with

or without stimulation (Figure S1D). Moreover, in the mouse T cell hybridoma 2B4, stimulation with anti-CD3ε+CD28 antibodies did not increase the association of EB1 with the TCR. Effective stimulation in these assays was confirmed by reprobing the membrane with a phosphospecific antibody, revealing that TCR triggering induced a clear increase in the tyrosine phosphorylation of CD3ζ (Figure S1E). Finally, CD3ζ homodimer was co-precipitated by EB1 immunoprecipitation in CH7C17 T cells activated or not with HA antigen (Figure 1E). These results indicate that EB1 interacts constitutively with the TCR in T cells, independently of their phosphorylation state.

EB1 localizes at the plus-ends of microtubules in the immune synapse.

The localization of EB1 during immune synapse formation in activated T cells was assessed in a model of antigen-specific presentation. Primary CD4+ T cells from OT-II transgenic mice were isolated and conjugated with TNF-α–activated, bone marrow-derived dendritic cells (DCs). In these conjugates, T cells are observed as small, round cells. Cell morphology and IS formation were monitored by F-actin staining. EB1 was detected at the tips of MTs in both the T cell and the DC. In the OVA-stimulated T cells, EB1 strongly decorated the ends of MT emerging from the polarized MTOC (yellow arrow, Figure 2A and Supplementary Figure S2A), being closely apposed to the cortical F-actin at the IS. This localization suggests a possible role of highly EB1-enriched MT plus-ends as docking structures for maintaining the MTOC at the IS. To further assess EB1 localization during IS formation, we conjugated human polyclonal, primary T lymphoblasts with either control or SEE-pulsed Raji B cells (antigen-presenting cell, APC; Figure 2B). In the absence of SEE, T lymphoblasts localize their MTOC at the uropod (U). In this condition, endogenous EB1 was clearly observed both at the MTOC (yellow arrow) and at points that

correspond to the ends of microtubules (white arrowheads). The confocal plane shown for SEE-stimulated conjugates reveals the polarized MTOC localized at the IS. The points of EB1 staining can be observed near the CD3ζ cluster. The 3D reconstructions of the boxed areas in merged images allow observation of different planes, from the internal MTOC area to the zone just beneath the plasma membrane, marked by CD3ζ. Points of EB1 staining are observed in all planes, co-localizing with CD3ζ-enriched intracellular clusters and partially co-localizing with CD3ζ in the more external planes of the 3D reconstruction (white arrows, right panels in Figure 2B).

We further analyzed EB1 localization during IS formation in centrosomes isolated by fractionation through sucrose gradients. GCP3 protein was used as a specific marker of centrosomal fractions (Bettencourt-Dias & Glover, 2007). Equivalent volumes of specific fractions were loaded on the gel, revealing an increased content of EB1 protein in the centrosomal fractions of activated T lymphocytes (Figure 2C). EB1 at the centrosome is essential to configure a radial array of microtubules (Askham et al, 2002). Indeed, the increase of EB1 in the centrosomal fractions points to an increase in the polymerization of microtubules from the centrosome. Therefore, EB1 localization in the plus-ends of microtubules and in the centrosome upon T cell activation suggest a role for EB1 in the regulation of microtubule dynamics at the IS.

EB1 guides microtubule dynamics at the immune synapse.

To explore the role of EB1 as a plus-end tracking protein at the IS, we analyzed whether MTs are actively polymerized at the IS. Growth of MTs from the polarized MTOC was detected in antigen-specific cell conjugates of CH7C17 Jurkat cells and HA-pulsed APCs using EB1-GFP, at imaging the confocal plane where the

MTOC localized at the interface with the APC (Figure 3A; Supplementary Movie S1). EB1-GFP has been previously used to enable tracking of MT growth by TIRF microscopy (Grigoriev & Akhmanova, 2010) during T cell spreading over an activating anti-CD3+anti-CD28 surface (Bunnell et al, 2001). In this system, the EB1-GFP-labeled MT plus tips appear very soon after cells make contact with the surface, and MTOC polarization (white arrow in Figure 3B; Supplementary Movie S2) is visualized within minutes. EB1-GFP is observed at the MTOC co-localizing with tubulin-Cherry rapidly upon T cell spreading (Supplementary Figure S2B). The irradiation of MTs is observed as points of EB1-GFP emanating from the translocated MTOC (Figure 3B; white arrows in Figure 3C; Supplementary Figure S2B and Movie S2-3). MTs can be visualized as filaments upon maximal projection of the time sequence on the XY plane (2D + t', Figure 3B-C). MT growth is also observed at the cell periphery during spreading, with some EB1-marked tips surrounding the adhesion area (red arrows in Figure 3B; Supplementary Movie S2) and even crossing over the central area (yellow arrow in Figure 3B; Supplementary Movie S2). These results point to MTOC polarization as a mechanism for facilitating EB1-driven polymerization of MTs at the IS, providing a dynamic meshwork for intracellular transport.

To analyze the relationship between MT dynamics and intracellular transport, CD3ζ dynamics was tracked with CD3ζ-Cherry, which was found both in microclusters attached to the activating surface and in vesicles (Supplementary Figure S3 and Movie S3). EB1-GFP and CD3ζ-Cherry are observed at the cell surface during spreading and CD3ζ-Cherry signal increases at a central cluster corresponding to the later localization of the polarized MTOC (Figure 3C and Supplementary Movie S4). When using a penetrance depth of 90 nm in TIRFM, microclusters are mainly

observed, whereas at 110 nm vesicles are also imaged (Figure 3C, Supplementary Figure S3 and Movie S3 and 4) and for a penetrance depth of 150 nm, vesicles were mainly on the focus plane (Figure 3D, Supplementary Movie S5). CD3ζ+ vesicles co-localized with the EB1-marked MT tips during T cell spreading over the activating surface (Figure 3D). These vesicles entered and exited the TIRF focal plane at sites of active MT growth (yellow and white arrowheads, respectively). These results indicate that CD3+ vesicles preferentially use the observed areas of high MT dynamics to move and accumulate.

EB1 controls the movement of CD3ζ-Cherry-containing vesicles at the IS.

To assess the function of EB1 in the movement of the CD3ζ-Cherry-enriched vesicles, EB1 was specifically knocked-down in CH7C17 T cells (Supplementary Figure S4). Tracking of vesicle movement by TIRFM in cells plated on stimulating surfaces revealed that movement of CD3ζ-Cherry vesicles at the central area of the T cell was impaired in EB1-depleted cells and that these vesicles were mostly displaced to the periphery (Figure 4A and Supplementary Movie S6). This is illustrated by projecting the time lapse on the XY plane (2D + t'), which details the areas where the CD3ζ+ vesicles have been moving (Figure 4B). The time projection on Figure 4C shows that the trajectories of the vesicles in EB1-silenced cells were irregular, in contrast with control cells. Therefore, these data indicate an EB1-dependent, specific control of CD3ζ vesicle movement at the IS. To further analyze the role of EB1 in CD3ζ positioning at the IS, EB1 expression was silenced in SEE-specific human T lymphoblasts and J77 Jurkat cells (Supplementary Figure S4B-C). Cell conjugates were formed with SEE-pulsed APCs, and analyzed for CD3ζ accumulation at the IS. Although in EB1-depleted cells CD3ζ can be found at the contact area with the APC (Supplementary Figure S5), its clustering at the central area of the IS is impaired

(Figure 4D; Supplementary Figure S5). Hence, CD3ζ was found at the periphery of the contact area, correlating with the observed trajectories of the vesicles in EB1-silenced cells. Indeed, the mean fluorescence intensity per area at the IS was decreased in EB1-silenced cells (Figure 4D).

EB1 regulates the interaction of the TCR and LAT/PLCγ1 signalosomes.

To further analyze CD3ζ behaviour at the IS, we used TIRF microscopy to analyse the movement of GFP-tagged LAT-enriched vesicles in control and EB1-silenced cells. When EB1 expression is reduced, the movement of LAT-GFP vesicles at the contact area with the activating surface is impaired (Figure 5A; Supplementary Movie S7-8). In control T cells LAT-GFP and CD3ζ-Cherry-enriched vesicles co-localized upon plating on the activating surface, but this was not seen in EB1-silenced cells (Figure 5B; Supplementary Figure S6 and Supplementary Movie S9-10). The analysis of the movement of vesicles that appear and disappear form the TIRF plane showed that not only vesicle encounter is reduced, but that their movement is less organized, as observed in the 3D reconstruction of XY planes and time frames (Figure 5B). Analysis of LAT in EB1-silenced T lymphoblasts revealed that LAT did not accumulate at the uropod as in control cells, which relates to the increase in the LAT accumulation at the cell-cell contact in non-stimulated conjugates (Supplementary Figure S7). Upon stimulation with SEE-pulsed APCs, LAT accumulation at the IS area was decreased in EB1-silenced cells, but not abrogated. Indeed, the relative fluorescence intensity of LAT in EB1-silenced cells was also reduced with respect to control cells, suggesting that the redistribution of LAT from intracellular compartments is poorly achieved in EB1 silenced cells (Supplementary Figure S7A-B). The relationship between CD3 and LAT was further explored through specific immunoprecipitation of CD3ζ in control T cells or EB1-silenced T cells (Figure 5C).

Using specific conditions to preserve the microtubular cytoskeleton upon cell lysis, we have observed a decrease in the LAT recovery with CD3ζ upon EB1 silencing. These results point to a role of EB1 in the organization of the IS. To analyze the activation state of T cells upon EB1 silencing, we analyzed the phosphorylation of the scaffold molecule LAT. Phosphorylation of LAT on residues Y132 and Y191 was impaired in EB1-silenced T cells upon activation with HA and SEE, compared with the level in control cells (Figure 6A). In contrast, the phosphorylation level of CD3ζ (Y83) and ZAP70 (Y493) in response to Ag (HA) or SEE activation was unaffected (Figure 6B-C). Stimulation of EB1-silenced T lymphoblasts with anti-CD3+anti-CD28 yielded similar results (Figure 6D). Signal propagation from the stimulated TCR to LAT thus seems to be prevented when EB1 is absent.

As a further test of the role of EB1 in T cell activation we examined the activation of PLCγ1 at the IS by confocal microscopy of T-APC conjugates. PLCγ1 activation was determined by monitoring phosphorylation of residue Y783 (Poulin et al, 2005). Activated PLCγ1 was clearly localized at the IS of control T lymphoblasts, but this accumulation was prevented by EB1 depletion (Figure 7A-B). This finding was corroborated by analysis of the timing of PLCγ1 phosphorylation upon TCR activation, which showed that the activation of PLCγ1 is defective in these cells (Figure 7C). This result correlates with the lack of phosphorylation of LAT at Y132 (Figure 6A and D), where PLCγ1 docks upon stimulation (Paz et al, 2001). These results support a role for EB1 in connecting the TCR and LAT signalosomes to allow signal propagation during T cell activation.

Discussion.

In this study, we report the role of the +TIP microtubule-associated protein EB1 in IS formation and T cell activation in cells of human and mouse origin. We identify a new function for EB1 in connecting the trajectories of signaling vesicles at the IS, allowing coordinated transfer of the activation signal from the TCR to the LAT signalosomes.

The microtubule network organized around the MTOC has historically been viewed as a static scaffold for vesicle movement in polarized secretion (Stinchcombe & Griffiths, 2007) or for specific signaling microclusters at the IS (Hashimoto-Tane et al; Lasserre et al, 2010). The microtubule network was also found to be important for maintaining the contact area of T cells with a stimulating surface (Bunnell et al, 2001). The dynamics of the tubulin cytoskeleton has been analyzed in T cells in terms of post-translational modifications, particularly acetylation of lysine 40 in the α-tubulin subunit, which marks a population of more stable microtubules (Serrador et al, 2004). Over-expression of histone-deacetylase 6 (HDAC6), which deacetylates acetylated α-tubulin, prevents localization of the TCR at the center of the IS and the translocation of the microtubule-organizing center (MTOC). CD3ζ (Serrador et al, 2004) and ZAP70 (Huby et al, 1995) signaling components of the TCR complex have been shown to associate with α-tubulin upon TCR stimulation, and this is prevented by chemical inhibition of HDAC6 (Serrador et al, 2004). A specific relationship is thus established between tubulin and the TCR complex during T cell activation. However, the specific growth of microtubules at the IS and the role of this process has not been addressed previously. We detected active and specific tubulin polymerization at the IS, paralleling the localized polymerization of actin (Gomez & Billadeau, 2008). Our data show that the centrosome of the activated T lymphocyte is

very active as a centre of tubulin polymerization (MTOC) upon TCR engagement, and its translocation to the IS facilitates the localization of newly polymerized microtubules to this active cellular location. These microtubules may serve to guide the trafficking of specific vesicles at the IS to the plasma membrane and from the plasma membrane to intracellular compartments since inhibition of MT growth through specific knock-down of EB1 (Komarova et al, 2009), prevents the correct movement of vesicles. Other foci of MT growth, unrelated to the centrosome and the Golgi Apparatus (Vinogradova et al, 2009), may contribute to intracellular traffic at the IS and further studies should elucidate their role.

EB1 is composed of two well-differentiated domains: a globular calponin-homology domain that encompasses the N-terminal half of the protein and binds to MTs, and a C-terminal homodimerization domain. In the EB1 homodimer, the C-terminal domain adopts a novel coiled-coil, four-helix bundle conformation. Our results show that EB1 interacts through this four-helix bundle domain with the ITAM of CD3ε and the ITAMs of CD3ζ. This interaction may underlie the ability of EB1-decorated MT plus ends to bind TCR-bearing vesicles, promoting their movement in and out of the IS-plane. Interestingly, the movement of the vesicles is erratic when EB1 expression is reduced, and corresponds to the localization of accumulated, peripheral clusters of TCR in fixed cell conjugates.

Our results reveal that signals from the TCR signalosome (Guy & Vignali, 2009) cannot propagate to the LAT/PLCγ1 cassette when EB1-dependent tracking of microtubules is disrupted, supporting the notion that a continuously-remodeled microtubular network is essential for the trafficking of vesicles at the IS. Moreover, TCR and LAT vesicles appear to be different and must encounter each other to allow the specific propagation of activation signals. These effects are very rapid and can be

observed readily after T cell activation, correlating with the described effect of HDAC6 on tubulin dynamics upon TCR engagement (Serrador et al, 2004). The backward trafficking to intracellular compartments of vesicles docked at microtubule plus-tips is in accord with a recently proposed model (Akhmanova & Hammer, 2010), in which dynein/dynactin molecular motors would drive movement toward the minus end of the microtubules (the centrosome). In this regard, EB1 C terminus ends with an acidic stretch that has been described as the binding site for $p150^{Glued}$, a dynactin subunit (Manna et al, 2008). Therefore, EB1 localized at microtubule plus-ends may help the interaction of TCR and thus CD3ζ-enriched vesicles with dynein/dynactin motors. A dynein/dynactin-driven movement would promote the movement of vesicles along microtubules toward their minus-end, the centrosome, where the Golgi is organized. The multivesicular bodies found at the IS (Calabia-Linares et al, 2011; Mittelbrunn et al, 2011) might also be the fate of the TCR-containing vesicles, on their way to recycling or degradation pathways. Early endosomal compartments may also be attained through microtubule driven trafficking (Nielsen et al, 1999).

The failure of MTOC translocation in dynein/dynactin-disrupted T cells of human origin (Martin-Cofreces et al, 2008) would prevent the tubulin polymerization at the IS observed here, preventing correct movement of vesicles toward intracellular compartments. The predicted outcome would be accumulation of TCR at the periphery of the IS instead of forming a central cluster, as observed (Martin-Cofreces et al, 2008). The tubulin cytoskeleton and related proteins therefore appear to be of critical importance for the formation of the IS and sustained T cell activation. In this regard, a recent report has identified casein kinase I δ (CKIδ) as an important kinase controlling MTOC translocation to the IS and microtubule growing. CKIδ can bind to EB1 and the region of CKIδ implicated in this interaction is required for MTOC

translocation (Zyss et al, 2011). Therefore, EB1 localization at the MTOC may be determined by CKIδ, and its plus-end tracking activity regulated by the kinase through phosphorylation to promote the microtubule growing observed herein. However, the lack of CKIδ does not affect IS architecture nor signaling (Zyss et al, 2011), which points to other complementary mechanisms to regulate EB1 function.

We found that vesicle movement is important for correct activation of signaling via LAT and PLCγ1. Phosphorylation of these proteins on key residues was decreased in EB1-silenced cells, even though the rate of phosphorylation of CD3ζ and ZAP70 was similar to control cells. LAT phosphorylation during T cell spreading and its correspondence with microclusters has been shown to be relevant during T cell activation (Campi et al, 2005). Indeed, the relative movement of LAT microclusters with respect to LAT vesicles has also been shown to be important for correct T cell activation (Purbhoo et al, 2010). Our results show that the coordinated movement and correct encounter between CD3ζ- and LAT-enriched vesicles is necessary for signal propagation from the TCR. This movement may help the relationship between the described protein islands for TCR and LAT (Lillemeier et al, 2010). The specific contribution of MTOC translocation to the localization of vesicles at the IS and subsequent microtubule polymerization warrants further research.

Material and Methods.

Cells, plasmids and cell transfection. All primary healthy donor samples were obtained after written consent, in accordance with the Declaration of Helsinki, and approved by the Hospital La Princesa Research Ethics Committee. Human T lymphoblasts were obtained from peripheral blood lymphocytes (PBLs) isolated from freshly prepared buffy coats. Buffy coats were subjected to gradient centrifugation on Histopaque-1077 from Sigma-Aldrich (St. Louis, MO, USA), followed by 2 rounds of plastic adherence. SEE-specific human T lymphoblasts were obtained as described (Ibiza et al, 2006). Vβ8+ Jurkat T cell clones (J77) and the lymphoblastoid Raji and Hom2 B cell lines were cultured in complete medium. HA-specific, Vβ3+ Jurkat T cells (CH7C17) were supplemented with 400 μg/ml hygromycin B and 4 μg/ml puromycin (Martin-Cofreces et al, 2008). T lymphoblasts were isolated by negative selection using the AutoMACS cell separation system (Miltenyi Biotec GmbH, Bergisch Gladbach, Germany). The cDNA encoding N-terminal GFP-linked EB1 was a kind gift from Anna Akhmanova (Utrecht University, The Netherlands). LAT-GFP was as described (Bonello et al, 2004). The indicated cDNAs were transiently transfected into T cells ($2x10^7$) with the Bio-Rad Gene Pulser II electroporation system. At 16 h post-transfection, viable T lymphoblasts, J77 or CH7C17 cells were isolated by centrifugation on a Ficoll-Hypaque gradient and conjugated with Raji (T lymphoblasts and J77 cells) or Hom2 cells (CH7C17 cells) for functional studies. EB1 silencing assays were performed as follows: J77 or CH7C17 T cells were electroporated with a shRNA plasmid encoding a specific 21 bp sequence against EB1 (GACATGACATGCTGGCCTGCG) or with the corresponding control plasmid encoding a negative sequence (TGGCATTGTCTTACCGCCTAT) (Genscript, Piscataway, NJ, USA), or instead with a double-stranded control siRNA or a specific

sequence against EB1 (CAGACAAGGUCAAGAAACU and CGUACGCGGAAUACUUCGA, respectively; Eurogentec, San Diego, CA, USA) at a final concentration of 2 μM per sample. Cells were then collected and the efficiency of gene silencing assessed by western blot. Cells were used for experiments on day three post-electroporation with shRNA or the day after electroporation with siRNA. For TIRFM analyses, cells were re-electroporated with shRNA and plasmids for LAT-GFP and/or CD3ζ-Cherry after 3 days of cell culture with 0.75 mg/ml G418 as selection antibiotic and used the following day.

Yeast two-Hybrid assay.

To characterize new CD3ε-interacting partners we used the yeast two-hybrid SOS-recruitment system (Gil et al, 2002). The sequence encoding the human CD3e cytoplasmic tail was amplified by PCR with end primers that add NcoI and SacI flanking restriction sites, and was cloned into the plasmid pSOS (Stratagene) to yield pSOS-CD3ε. As a bait we used the construct pSOS-CD3ε Tandem containing two copies in tandem, head to tail, of the cytoplasmic tail of CD3ε. The control constructs pSOS-Mafb, pMyr-Mafb and pMyr-LamC were provided by Stratagene. The bait construct was transfected in the cdc25 yeast mutant together with a human spleen cDNA library made in the pMyr vector (Stratagene) and the transfectants (3x106) were selected at the restrictive temperature (37ºC) in a manner dependent of galactose, and not glucose, as a carbon source. Of the 319 resulting colonies, 304 were discarded as revertants of the cdc25 mutation since they grew in the presence of glucose. The pMyr plasmid was isolated of the remaining 15 clones and assayed in regard to their ability to promote the growth in galactose at 37ºC in the presence of the empty pSOS vector. Only two clones did not grow in these

conditions, one contained a cDNA encoding for Nck-β (Gil et al, 2002); the other for the last 82 amino acids of EB1.

Antibodies and reagents. T3b (anti-human-CD3) and was produced in the laboratory. Rabbit polyclonal Ab 448 (anti-human-CD3ζ) has been described previously (San Jose et al, 1998). Anti–human Vβ8 was from BD Biosciences/Clontech (San Jose, CA, USA). Unconjugated and FITC-conjugated anti–α-tubulin, phalloidin and GCP3 rabbit polyclonal were from Sigma-Aldrich (St. Louis, MO). Anti-LAT was from Santa Cruz Biotechnology, Inc. (Santa Cruz, CA, USA). Anti–phospho-LAT (Y191) was from Millipore (Billerica, MA, USA), and anti–phospho-LAT (Y132) was from Abcam (Cambridge, MA, USA). Anti–phospho-PLCγ-1 (Y783), anti–PLCγ-1 and anti–phospho-PKCθ (T538) were from Cell Signaling Technology (Danvers, MA, USA). Anti-phospho-CD3z (Y83) was from Epitomics (Burlingame, CA, USA).

Human fibronectin and poly-L-lysine (PLL) were from Sigma-Aldrich, SEE from Toxin Technology (Sarasota, FL, USA), puromycin from InvivoGen (San Diego, CA, USA), and hygromycin B from Roche Diagnostics GmbH (Penzberg, Germany). Anti-Erk 1/2 and the fluorescent secondary antibodies (Alexa 568 and 647, and rhodamine red X) and cell trackers (7-amino-4-chloromethylcoumarin [CMAC], 5-(and-6)-(((4-chloromethyl) benzoyl) amino) tetramethylrhodamine [CMTMR]) were obtained from Invitrogen (Carlsbad, CA, USA). Propidium Iodide was from Sigma-Aldrich. All other reagents were of the purest grade available.

Cell conjugate formation and immunofluorescence analysis. Raji B cells were loaded with the blue fluorescent cell tracker CMAC. Cells were then incubated in HBSS for 30 min with or without 0.5 μg/ml SEE, centrifuged at low speed, and allowed to form conjugates with J77 Jurkat cells or SEE-CD4 human primary T cells

during incubation for 20 min at 37°C. Hom2 cells were also loaded with CMAC, incubated for 2 h with 50 μg/ml HA peptide, and allowed to form conjugates with CH7C17 cells. In these assays, the T cells ($2X10^5$) were mixed with an equal number of APCs in a final volume of 80 μl, gently resuspended, and plated onto slides coated with PLL (Jurkat) or FN (CH7C17). Cells were fixed with a mix of paraformaldehyde and methanol for 4 min at -20 ºC and permeabilized when needed for 5 min in 2% paraformaldehyde and 0.2% Triton X-100 in PHEM/sacarose, blocked and stained with the indicated Abs. Stained cells were mounted in a mowiol-based mounting solution (ProLong Gold antifade reagent; Invitrogen) and observed under a confocal laser scanning unit (TCS SP5; Leica) attached to an inverted epifluorescence microscope (DMI6000; Leica) fitted with an HCX PL APO 63X/1.40-0.6 oil objective. Images were acquired and processed with accompanying confocal software (LCS; Leica) or WCIF ImageJ (http://rsbweb.nih.gov/ij/). 3D analysis and maximal projections of the T cell–APC contact area were generated with ImageJ to obtain a z stack projection. Figures were composed with Photoshop CS4.

Analysis of CD3ζ, LAT and PLCγ1 accumulation at the T-APC contact area. T-APC conjugates were formed, fixed and analyzed by confocal imaging as indicated above and images were analyzed with ImageJ. We assumed that protein accumulation was homogeneous in the APC when present, with no additional accumulation at the contact zone with the T cell. For quantification in individual ISs we used a home-made plugin for ImageJ (http://rsbweb.nih.gov/ij/) called "*Synapse Measures*". By comparing fluorescence signals from multiple regions of the T cell, APC, IS, and background fluorescence, the program yields accurate measurements of localized immunofluorescence. A detailed description of *Synapse Measures*, including the algorithms used, is described (Calabia-Linares et al, 2011).

Time-lapse fluorescence confocal microscopy and total internal reflection fluorescence microscopy (TIRFM). Raji APCs ($5x10^5$; SEE-pulsed or unpulsed) were allowed to adhere to FN coated coverslips in Attofluor open chambers (Invitrogen) at 37ºC in a 5% CO_2 atmosphere. The cells were maintained in 1 ml HBSS (2% BSA). T cells were added (1:1 ratio) and a series of fluorescence and differential interference contrast frames were captured using a TCS SP5 confocal laser scanning unit attached to an inverted epifluorescence microscope (DMI6000) fitted with an HCX PL APO 63x/1.40-0.6 oil objective. Images were acquired and processed with the accompanying confocal software (LCS; Leica). Premiere 6.0 software (Adobe) was used to generate QuickTime videos (Apple).

For TIRFM, T cells transfected with CD3ζ-Cherry, LAT-GFP, and control or shEB1 plasmid were allowed to settle onto CD3 plus CD28 coated glass bottomed microwell dishes, No 1.5 (Mattek; Ashland, MA, US). Recording was initiated 3 minutes after cells were platted and cells were visualized with a Leica AM TIRF MC M mounted on a Leica DMI 6000B microscope coupled to an Andor-DU8285_VP-4094 camera. Images were acquired with a HCX PL APO 100.0x1.46 OIL objective and processed with the accompanying confocal software (LCS; Leica). For vesicle tracking, penetrance was 150 or 250 nm for both laser channels (488 and 561 nm) with same objective angle. Synchronization was performed through the Leica software.

GST-pull down, immunoprecipitation, centrosomal isolation and immunoblotting. For GST-pull down, corresponding recombinant GST-protein were added to cell lysates and pull down performed as described (Urzainqui et al, 2002). For immunoprecipitation, T cells were stimulated with corresponding Ag or Sag-pulsed APCs (ratio 1:5) or antibodies (anti-CD3 or anti-CD3 + anti-CD28) for the

indicated times and lysed in 20 mM Tris-HCl, pH 7.5, 150 mM NaCl buffer containing 1% Brj96 and phosphatase and protease inhibitors in non-reducing conditions. Anti-HA tag antibody, anti-CD3ζ rabbit anti-serum or anti-EB1 antibody were used for immunoprecipitation. For LAT and CD3ζ co-immunoprecipitation, cells were silenced for EB1 and stimulated or not with anti-(CD3ε+CD28) antibody-coated beads. The complete procedure was performed at room temperature. Cells were lysed on PHEM buffer (60 mM PIPES, 25 mM Hepes, 5 mM EGTA, 2 mM MgCl2) with 0.33% Brij 96v supplemented with protease and phosphatase inhibitors. Preclearing and antibody recovery was performed using the Protein-G magnet beads from Millipore. Anti-CD3ζ rabbit anti-serum was used for immunoprecipitation during 2 h. Blots were revealed using True Blot reagent for detection of primary antibodies. Centrosomal isolation was performed from control or anti-CD3-stimulated CH7C17 T cells as described (Bornens & Moudjou, 1999). For analysis of protein phosphorylation during formation of the IS, Raji or Hom2 cells (1×10^6) were preloaded with 0.5 μg/ml SEE or 50 μg/ml HA peptide at 37°C for 30 min or 2 h and mixed with 5 x 10^6 Jurkat or CH7C17 cells at 37°C, respectively. After incubation, cells were lysed at 4°C for 40 min in 50 mM Tris-HCl, pH 7.5, containing 1% NP-40, 0.2% Triton X-100, 150 mM NaCl, and phosphatase and protease inhibitors. Cell lysates were spun at 2500 *g* for 10 min to remove cell debris and nuclei. GST-pull downs, immunoprecipitates, centrosomal fractions and whole lysates were analyzed by SDS-PAGE, transferred to nitrocellulose membranes, and probed with the indicated antibodies in TBS–Tween 20. Bound antibodies were reacted with HRP secondary antibodies, and membranes were developed by enhanced chemiluminescence with SuperSignal West Pico or Femto chemiluminescent

substrate (Pierce). Densitometric analyses were performed with ImageGauge 3.46 software (Fujifilm).

Statistical analysis. Data were tested for normality using the D'Agostino-Pearson omnibus normality test, or the Kolmogorov-Smirnov test when the sample was small. Differences between means were tested by Student's *t* test for normal data, while non-normal data were analyzed by the Mann-Whitney test. Two-tailed ANOVA was used for grouped data, followed by Bonferroni posttest. GraphPad Prism software was used for statistical analyses.

Online Supplemental material. Videos 1 to 10, related to the main figures or the corresponding supplemental figures in the manuscript are available on-line. Videos 1-2 reflects EB1 localization at the immunological synapse. Videos 3-6, relationship between EB1 and CD3. Videos 7-8, relationship between EB1 and LAT. Videos 9-10, correlation between LAT and CD3 vesicles depending on EB1 presence.

Acknowledgements

We thank S. Bartlett for editorial support and critical reading of the manuscript. This work was supported by grants from Spanish Ministry of Science and Innovation (SAF2011-25834 to FSM, SAF2010-14912 to BA and grants to FB and NBMC), INDISNET S2011/BMD-2332 to FSM and BA from Comunidad de Madrid and ERC-2011-AdG 294340-GENTRIS. The Centro Nacional de Investigaciones Cardiovasculares (CNIC, Spain) is supported by the Spanish Ministry of Science and Innovation and the Pro-CNIC Foundation.

Author contribution

NBMC, FB, BA and FSM designed experimentation and analyzed results; NBMC, FB, MJ, DG and AM collected and analyzed the data; NBMC made the figures and wrote the manuscript with input from FB, BA and FSM.

Conflict of interest

Authors declare that they have no conflict of interest.

References

Akhmanova A, Hammer JA, 3rd (2010) Linking molecular motors to membrane cargo. *Curr Opin Cell Biol* **22:** 479-487

Akhmanova A, Steinmetz MO (2008) Tracking the ends: a dynamic protein network controls the fate of microtubule tips. *Nat Rev Mol Cell Biol* **9:** 309-322

Askham JM, Vaughan KT, Goodson HV, Morrison EE (2002) Evidence that an interaction between EB1 and p150(Glued) is required for the formation and maintenance of a radial microtubule array anchored at the centrosome. *Mol Biol Cell* **13:** 3627-3645

Baixauli F, Martin-Cofreces NB, Morlino G, Carrasco YR, Calabia-Linares C, Veiga E, Serrador JM, Sanchez-Madrid F (2011) The mitochondrial fission factor dynamin-related protein 1 modulates T-cell receptor signalling at the immune synapse. *EMBO J* **30:** 1238-1250

Bettencourt-Dias M, Glover DM (2007) Centrosome biogenesis and function: centrosomics brings new understanding. *Nat Rev Mol Cell Biol* **8:** 451-463

Bonello G, Blanchard N, Montoya MC, Aguado E, Langlet C, He HT, Nunez-Cruz S, Malissen M, Sanchez-Madrid F, Olive D, Hivroz C, Collette Y (2004) Dynamic recruitment of the adaptor protein LAT: LAT exists in two distinct intracellular pools and controls its own recruitment. *J Cell Sci* **117:** 1009-1016

Bornens M, Moudjou M (1999) Studying the composition and function of centrosomes in vertebrates. *Methods Cell Biol* **61:** 13-34

Bunnell SC, Kapoor V, Trible RP, Zhang W, Samelson LE (2001) Dynamic actin polymerization drives T cell receptor-induced spreading: a role for the signal transduction adaptor LAT. *Immunity* **14:** 315-329

Calabia-Linares C, Robles-Valero J, De La Fuente H, Perez-Martínez M, Martin-Cofreces NB, Alfonso-Pérez M, Gutierrez-Vázquez C, Mittelbrunn M, Ibiza S, Urbano-Olmos FR, Aguado-Ballano C, Sánchez-Sorzano CO, Sánchez-Madrid F, Veiga E (2011) Endosomal clathrin drives actin accumulation at the immunological synapse. . *J Cell Sci* **124:** 820-830

Campi G, Varma R, Dustin ML (2005) Actin and agonist MHC-peptide complex-dependent T cell receptor microclusters as scaffolds for signaling. *J Exp Med* **202:** 1031-1036

Etienne-Manneville S (2010) From signaling pathways to microtubule dynamics: the key players. *Curr Opin Cell Biol* **22:** 104-111

Gil D, Schamel WW, Montoya M, Sanchez-Madrid F, Alarcon B (2002) Recruitment of Nck by CD3 epsilon reveals a ligand-induced conformational change essential for T cell receptor signaling and synapse formation. *Cell* **109:** 901-912

Gomez TS, Billadeau DD (2008) T cell activation and the cytoskeleton: you can't have one without the other. *Adv Immunol* **97:** 1-64

Grigoriev I, Akhmanova A (2010) Microtubule dynamics at the cell cortex probed by TIRF microscopy. *Methods Cell Biol* **97:** 91-109

Guy CS, Vignali DA (2009) Organization of proximal signal initiation at the TCR:CD3 complex. *Immunol Rev* **232:** 7-21

Hashimoto-Tane A, Yokosuka T, Sakata-Sogawa K, Sakuma M, Ishihara C, Tokunaga M, Saito T (2011) Dynein-driven transport of T cell receptor microclusters regulates immune synapse formation and T cell activation. *Immunity* **34:** 919-931

Huby RD, Carlile GW, Ley SC (1995) Interactions between the protein-tyrosine kinase ZAP-70, the proto-oncoprotein Vav, and tubulin in Jurkat T cells. *J Biol Chem* **270:** 30241-30244

Huse M, Quann EJ, Davis MM (2008) Shouts, whispers and the kiss of death: directional secretion in T cells. *Nat Immunol* **9:** 1105-1111

Ibiza S, Victor VM, Bosca I, Ortega A, Urzainqui A, O'Connor JE, Sanchez-Madrid F, Esplugues JV, Serrador JM (2006) Endothelial nitric oxide synthase regulates T cell receptor signaling at the immunological synapse. *Immunity* **24:** 753-765

Komarova Y, De Groot CO, Grigoriev I, Gouveia SM, Munteanu EL, Schober JM, Honnappa S, Buey RM, Hoogenraad CC, Dogterom M, Borisy GG, Steinmetz MO, Akhmanova A (2009) Mammalian end binding proteins control persistent microtubule growth. *J Cell Biol* **184:** 691-706

Lasserre R, Charrin S, Cuche C, Danckaert A, Thoulouze MI, de Chaumont F, Duong T, Perrault N, Varin-Blank N, Olivo-Marin JC, Etienne-Manneville S, Arpin M, Di Bartolo V, Alcover A (2010) Ezrin tunes T-cell activation by controlling Dlg1 and microtubule positioning at the immunological synapse. *EMBO J* **29:** 2301-2314

Li R, Gundersen GG (2008) Beyond polymer polarity: how the cytoskeleton builds a polarized cell. *Nat Rev Mol Cell Biol* **9:** 860-873

Lillemeier BF, Mortelmaier MA, Forstner MB, Huppa JB, Groves JT, Davis MM (2010) TCR and Lat are expressed on separate protein islands on T cell membranes and concatenate during activation. *Nat Immunol* **11:** 90-96

Lowin-Kropf B, Shapiro VS, Weiss A (1998) Cytoskeletal polarization of T cells is regulated by an immunoreceptor tyrosine-based activation motif-dependent mechanism. *J Cell Biol* **140:** 861-871

Manna T, Honnappa S, Steinmetz MO, Wilson L (2008) Suppression of microtubule dynamic instability by the +TIP protein EB1 and its modulation by the CAP-Gly domain of p150glued. *Biochemistry* **47:** 779-786

Martin-Cofreces NB, Robles-Valero J, Cabrero JR, Mittelbrunn M, Gordon-Alonso M, Sung CH, Alarcon B, Vazquez J, Sanchez-Madrid F (2008) MTOC translocation modulates IS formation and controls sustained T cell signaling. *J Cell Biol* **182:** 951-962

Martin-Cofreces NB, Sancho D, Fernandez E, Vicente-Manzanares M, Gordon-Alonso M, Montoya MC, Michel F, Acuto O, Alarcon B, Sanchez-Madrid F (2006) Role of Fyn in the rearrangement of tubulin cytoskeleton induced through TCR. *J Immunol* **176:** 4201-4207

Mittelbrunn M, Gutierrez-Vazquez C, Villarroya-Beltri C, Gonzalez S, Sanchez-Cabo F, Gonzalez MA, Bernad A, Sanchez-Madrid F (2011) Unidirectional transfer of microRNA-loaded exosomes from T cells to antigen-presenting cells. *Nat Commun* **2:** 282

Nielsen E, Severin F, Backer JM, Hyman AA, Zerial M (1999) Rab5 regulates motility of early endosomes on microtubules. *Nat Cell Biol* **1:** 376-382

Paz PE, Wang S, Clarke H, Lu X, Stokoe D, Abo A (2001) Mapping the Zap-70 phosphorylation sites on LAT (linker for activation of T cells) required for recruitment and activation of signalling proteins in T cells. *Biochem J* **356:** 461-471

Poulin B, Sekiya F, Rhee SG (2005) Intramolecular interaction between phosphorylated tyrosine-783 and the C-terminal Src homology 2 domain activates phospholipase C-gamma1. *Proc Natl Acad Sci U S A* **102:** 4276-4281

Purbhoo MA, Liu H, Oddos S, Owen DM, Neil MA, Pageon SV, French PM, Rudd CE, Davis DM (2010) Dynamics of subsynaptic vesicles and surface microclusters at the immunological synapse. *Sci Signal* **3:** ra36

San Jose E, Sahuquillo AG, Bragado R, Alarcon B (1998) Assembly of the TCR/CD3 complex: CD3 epsilon/delta and CD3 epsilon/gamma dimers associate indistinctly with both TCR alpha and TCR beta chains. Evidence for a double TCR heterodimer model. *Eur J Immunol* **28:** 12-21

San Jose E, Alarcon B (1999) Receptor engagement transiently diverts the T cell receptor heterodimer from a constitutive degradation pathway. *J Biol Chem* **274**: 33740-6

Schamel WW, Risueno RM, Minguet S, Ortiz AR, Alarcon B (2006) A conformation- and avidity-based proofreading mechanism for the TCR-CD3 complex. *Trends Immunol* **27:** 176-182

Serrador JM, Cabrero JR, Sancho D, Mittelbrunn M, Urzainqui A, Sanchez-Madrid F (2004) HDAC6 deacetylase activity links the tubulin cytoskeleton with immune synapse organization. *Immunity* **20:** 417-428

Sigalov AB (2006) Immune cell signaling: a novel mechanistic model reveals new therapeutic targets. *Trends Pharmacol Sci* **27**: 518-24

Stinchcombe JC, Griffiths GM (2007) Secretory mechanisms in cell-mediated cytotoxicity. *Annu Rev Cell Dev Biol* **23:** 495-517

Tirnauer JS, Bierer BE (2000) EB1 proteins regulate microtubule dynamics, cell polarity, and chromosome stability. *J Cell Biol* **149:** 761-766

Urzainqui A, Serrador JM, Viedma F, Yanez-Mo M, Rodriguez A, Corbi AL, Alonso-Lebrero JL, Luque A, Deckert M, Vazquez J, Sanchez-Madrid F (2002) ITAM-based interaction of ERM proteins with Syk mediates signaling by the leukocyte adhesion receptor PSGL-1. *Immunity* **17:** 401-412

van der Merwe PA, Dushek O (2011) Mechanisms for T cell receptor triggering. *Nat Rev Immunol* **11:** 47-55

Vinogradova T, Miller PM, Kaverina I (2009) Microtubule network asymmetry in motile cells: role of Golgi-derived array. *Cell Cycle* **8:** 2168-2174

Zyss D, Ebrahimi H, Gergely F (2011) Casein kinase I delta controls centrosome positioning during T cell activation. *J Cell Biol* **195:** 781-797

Figure Legends.

Figure 1. ITAM-dependent interaction of CD3 with EB1. (A), Pull-down of HA-tagged CD3 subunits with full-length GST-EB1 in co-transfected COS cells. A representative experiment out of 3 independent experiments is shown. **(B)** Co-immunoprecipitation of HA-tagged, full-length EB1 with chimeras of the CD8a extracellular region and the depicted CD3 ITAM sequences. A representative experiment out of 3 independent experiments is shown. **(C)** Pull down with the depicted GST-EB1 C-terminal regions of CD3ζ from the 2B4 mouse T cell hybridoma and human Jurkat T cell lines. A representative experiment out of 5 independent experiments is shown. **(D)** Co-immunoprecipitation of EB1 and surface TcR/CD3 in Jurkat T cells. Biotinylated cells were lysed and subjected to immunoprecipitation with anti-EB1 or CD3ζ antibodies. Samples were analyzed in the same gel. The image shown in the figure is a composition from two autoradiographs of different time exposure. **(E)** Co-immunoprecipitation of EB1 with anti-CD3ζ in the human CH7C17 T cell line stimulated as indicated with HA-pulsed Hom2 cells (ratio 10:1) in non-reducing conditions; C-, immunoprecipitation with control antibody. A representative experiment out of 4 independent experiments is shown.

Figure 2. EB1 localizes at the plus-end tips of microtubules in the IS. (A) Conjugates formed between primary mouse CD4+ T cells from OT-II transgenic mice and TNF-α–stimulated, bone marrow-derived dendritic cells (DC). DCs were pulsed with peptide (OVA) or not (-). After incubation for 30 minutes, conjugates were fixed and stained for the indicated antibodies. Left panels show DIC images (DC blue-

stained with CMAC) and F actin staining. Bar, 10μm. Main panels, a single confocal plane from a Z-stack corresponding to the boxed area in the DIC image. Right panels, orthogonal projections of the indicated MTOCs (dashed lines). Representative cell conjugates from out of 4 independent experiments is shown. **(B)** Fluorescence images from a magnification of the conjugate boxed in the DIC image. Raji APC in blue; DIC, bright field image; U, uropod. Bar, 10μm. Upper panels show maximal projections of a confocal Z-stack showing a SEE-specific T lymphoblast conjugated with a control Raji APC (No SEE). Yellow arrow, MTOC; white arrowheads, microtubule tips. Lower panels show confocal planes from a Z-stack of stimulated T lymphoblasts showing their polarized MTOCs at the contact area with the APC (SEE-pulsed Raji B cells). After incubation for 30 minutes, conjugates were fixed and immunostained for α-tubulin (magenta), EB1 (red) and CD3 (green). Right panels show 3D reconstructions of boxed area in the merged image. The resulting planes are ordered from the T cell intracellular region (the MTOC in the case of the SEE-stimulated cell) toward the T cell plasma membrane in close contact with the APC. White arrows, co-localization of EB1 and CD3ζ. Representative cell conjugates from out of at least 3 independent experiments are shown. **(C)** Sucrose gradient fractionation of centrosomes (GCP3 positive fractions) showing EB1 enrichment in anti-CD3 stimulated T cells. Right panel shows the protein content from cell extracts. TL, total lysates; Cyt, cytosolic lysates; SC, sucrose cushion. Left panel shows the isolation of centrosomes. F, sucrose fractions. A representative experiment out of 3 independent experiments is shown.

Figure 3. Microtubule dynamics are driven by EB1 at the IS. (A) EB1-GFP–expressing CH7C17 T cells were conjugated with HA-pulsed APCs and tracked by

confocal fluorescence microscopy. A single confocal plane is shown. Images were taken every 2 s. The merged image at the right shows DIC and GFP fluorescence (green). *, HA-loaded Hom2 B cell. A representative cell conjugate from out of at least 3 independent experiments is shown. **(B)** EB1-GFP–expressing CH7C17 cells were allowed to settle on anti-CD3 plus anti-CD28 coated glass-bottomed chambers and images were taken every 500 ms by TIRF microscopy at a penetrance of 150 nm. A representative cell from out of 3 independent experiments is shown. **(C)** Jurkat T cells expressing EB1-mGFP (green) and CD3ζ-mCherry (red) were treated as in b and analyzed by TIRFM. Images were taken every 99 ms at a penetrance of 90 nm. White arrow, centrosome. Bar, 5 μm. A representative cell from out of at least 3 independent experiments is shown. **(D)** Jurkat T cells co-expressing EB1-GFP (green) and CD3ζ-Cherry (red) were plated on anti-CD3 plus anti-CD28 coated glass-bottomed chambers and analyzed by TIRFM. Images were taken every 1 s at a penetrance of 150 nm. The central panel shows magnified views of a time-lapse sequence of the boxed region between 1 s (left) and 40 s (right). Yellow arrowheads: vesicles appearing at the TRIF plane. White arrowheads: vesicles disappearing from the TIRF plane. White arrows: CD3ζ microclusters.

Figure 4. EB1 regulates the trafficking of CD3ζ-bearing vesicles at the IS. (A) shRNA-transfected (control or EB1) Jurkat T cells expressing CD3ζ-Cherry were plated on anti-CD3 plus anti-CD28 coated glass-bottomed chambers and analyzed by TIRFM. Images were taken every 500 ms at a penetrance of 110 nm. A representative cell out of at least 4 independent experiments is shown. **(B)** Maximal Z projections of the time-lapse sequences, summarizing vesicle movement in the XY plane (2D + t'). **(C)** Trajectory characteristics are revealed by the maximal projection of the X plane

on tY plane. **(D)** Images showing a single confocal plane (IS plane) corresponding to control (upper panel) or EB1-silenced (EB1 KD, lower panel) T lymphoblasts conjugated with SEE-pulsed Raji cells. Cells were mixed and cultured for 30 minutes, fixed and stained with the indicated antibodies. The graph to the right plots the distribution of intensity/area of CD3ζ at the IS. Data are means +/- SD from 3 independent experiments. (P, Mann-Whitney test).

Figure 5. Signal propagation at the IS is regulated by EB1. (A) LAT-GFP dynamics in control and EB1-silenced cells analyzed by TIRFM as in Figure 4A. Images were taken every 33 (control) or 51 ms (EB1 KD) at a penetrance of 150 nm. A representative cell from out of 4 independent experiments is shown. **(B)** Analysis of LAT-GFP and CD3ζ-Cherry dynamics in control and EB1-silenced cells by TIRFM as in Figure 3D. Images were taken every 2s at a penetrance of 250 nm. A single time frame is showed, as well as a 3D reconstruction of time vs XY planes. Graph, vesicle encounter at the TIRFM plane. Vesicles from 100 time frames were analyzed from out of 11 cells for trajectories from 5 different experiments. Images were processed for dynamics and co-localization with Imaris software (**, $P<0.05$; ***, $P<0.001$; two-tailed ANOVA followed by Bonferroni posttest). **(C)** Co-immunoprecipitation of CD3ζ and LAT in control and EB1-silenced cells. Cells were stimulated or not with anti-CD3ε+anti-CD28 antibodies.

Figure 6. Signal activation at the IS is regulated by EB1. (A) Western blot showing defective LAT activation in EB1-silenced cells CH7C17 or J77 Jurkat T cells stimulated with HA-specific peptide or SEE for the indicated times. Graphs, mean +/- SEM from 5 and 6 different experiments, respectively (*, $P<0.05$; **,

P<0.01. Two-tailed ANOVA followed by Bonferroni posttests) **(B-C)** Western blots showing phosphorylation of CD3ζ **(B)** and ZAP70 **(C)** in control and EB1-silenced CH7C17 or J77 Jurkat T cells stimulated with HA- or SEE-specific peptide for the indicated times. Graphs, mean +/- SEM (differences were considered not significant after a two-tailed ANOVA analysis followed by Bonferroni posttests; Y83: N=9 (HA), N=5 (SEE); Y493: N=4 (HA); N=3 (SEE)). **(D)** Phosphorylation of CD3ζ and LAT in control and EB1-silenced T lymphoblasts plated on anti-CD3+anti-CD28 antibodies. A representative experiment out of at least 3 independent experiments is shown. Graphs, mean +/- SEM from 3 different experiments (*, P<0.05; two-tailed ANOVA followed by Bonferroni posttests).

Figure 7. PLCγ1 activation and clustering at the IS depends on EB1. **(A)** Control and EB1-silenced human T lymphoblasts were conjugated with SEE-pulsed Raji APCs, fixed and processed for immunofluorescence with the indicated antibodies. PLCγ1 activation was detected with the phospho-specific antibody PLCγ1Y783. Bar, 10 μm. Asterisks mark SEE-pulsed Raji B cells. A representative cell conjugate out of at least 3 independent experiments is shown. **(B)** Scatter plot of the signal ratio for PLC1γY783 at the IS compared with the rest of the cell. Means +/- SD from 3 independent experiments are depicted. Data were analyzed with Mann-Whitney test. **(C)** Western blot showing the effect of EB1 knockdown on the timing of PLCγ1 Y783 phosphorylation in CH7C17 Jurkat T cells stimulated with HA specific peptide and in T lymphoblasts stimulated with SEE (*, P<0.05, ***, P<0.001. Two-tailed ANOVA followed by Bonferroni posttests. N=4 (HA) and N=3 (SEE)).

Figure 1

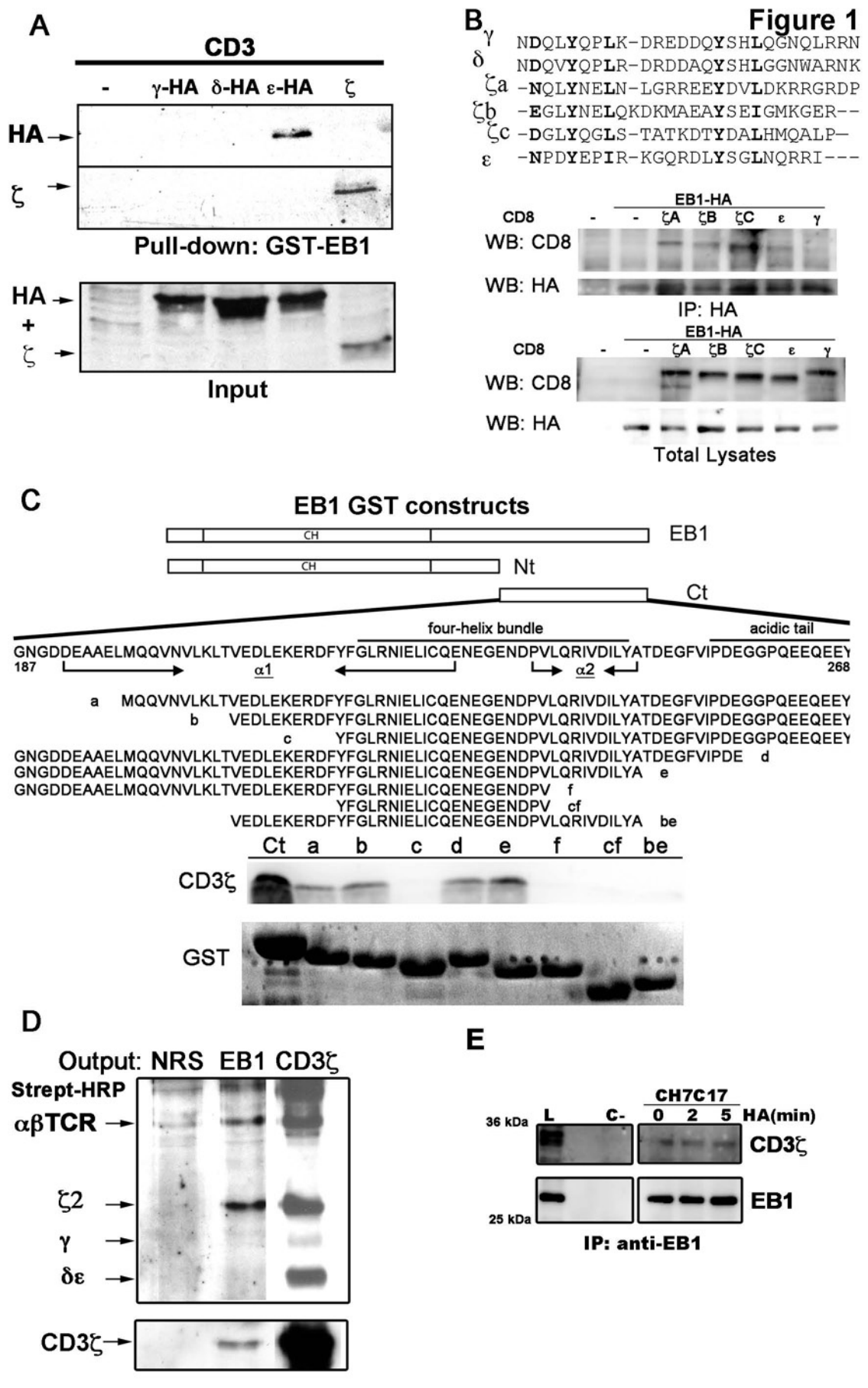
A
CD3
- γ-HA δ-HA ε-HA ζ
HA
ζ
Pull-down: GST-EB1
HA + ζ
Input
B
γ NDQLYQPLK-DREDDQYSHLQGNQLRRN
δ NDQVYQPLR-DRDDAQYSHLGGNWARNK
ζa -NQLYNELN-LGRREEYDVLDKRRGRDP
ζb -EGLYNELQKDKMAEAYSEIGMKGER--
ζc -DGLYQGLS-TATKDTYDALHMQALP—
ε -NPDYEPIR-KGQRDLYSGLNQRRI---
EB1-HA
CD8 - - ζA ζB ζC ε γ
WB: CD8
WB: HA
IP: HA
EB1-HA
CD8 - - ζA ζB ζC ε γ
WB: CD8
WB: HA
Total Lysates
C
EB1 GST constructs
CH
EB1
CH
Nt
Ct
four-helix bundle
acidic tail
GNGDDEAAELMQQVNVLKLTVEDLEKERDFYFGLRNIELICQENEGENDPVLQRIVDILYATDEGFVIPDEGGPQEEQEEY
187
α1
α2
268
a MQQVNVLKLTVEDLEKERDFYFGLRNIELICQENEGENDPVLQRIVDILYATDEGFVIPDEGGPQEEQEEY
b VEDLEKERDFYFGLRNIELICQENEGENDPVLQRIVDILYATDEGFVIPDEGGPQEEQEEY
c YFGLRNIELICQENEGENDPVLQRIVDILYATDEGFVIPDEGGPQEEQEEY
GNGDDEAAELMQQVNVLKLTVEDLEKERDFYFGLRNIELICQENEGENDPVLQRIVDILYATDEGFVIPDE d
GNGDDEAAELMQQVNVLKLTVEDLEKERDFYFGLRNIELICQENEGENDPVLQRIVDILYA e
GNGDDEAAELMQQVNVLKLTVEDLEKERDFYFGLRNIELICQENEGENDPV f
YFGLRNIELICQENEGENDPV cf
VEDLEKERDFYFGLRNIELICQENEGENDPVLQRIVDILYA be
Ct a b c d e f cf be
CD3ζ
GST
D
Output: NRS EB1 CD3ζ
Strept-HRP
αβTCR
ζ2
γ
δε
CD3ζ
E
CH7C17
36 kDa L C- 0 2 5 HA(min)
CD3ζ
EB1
25 kDa
IP: anti-EB1

Figure 2

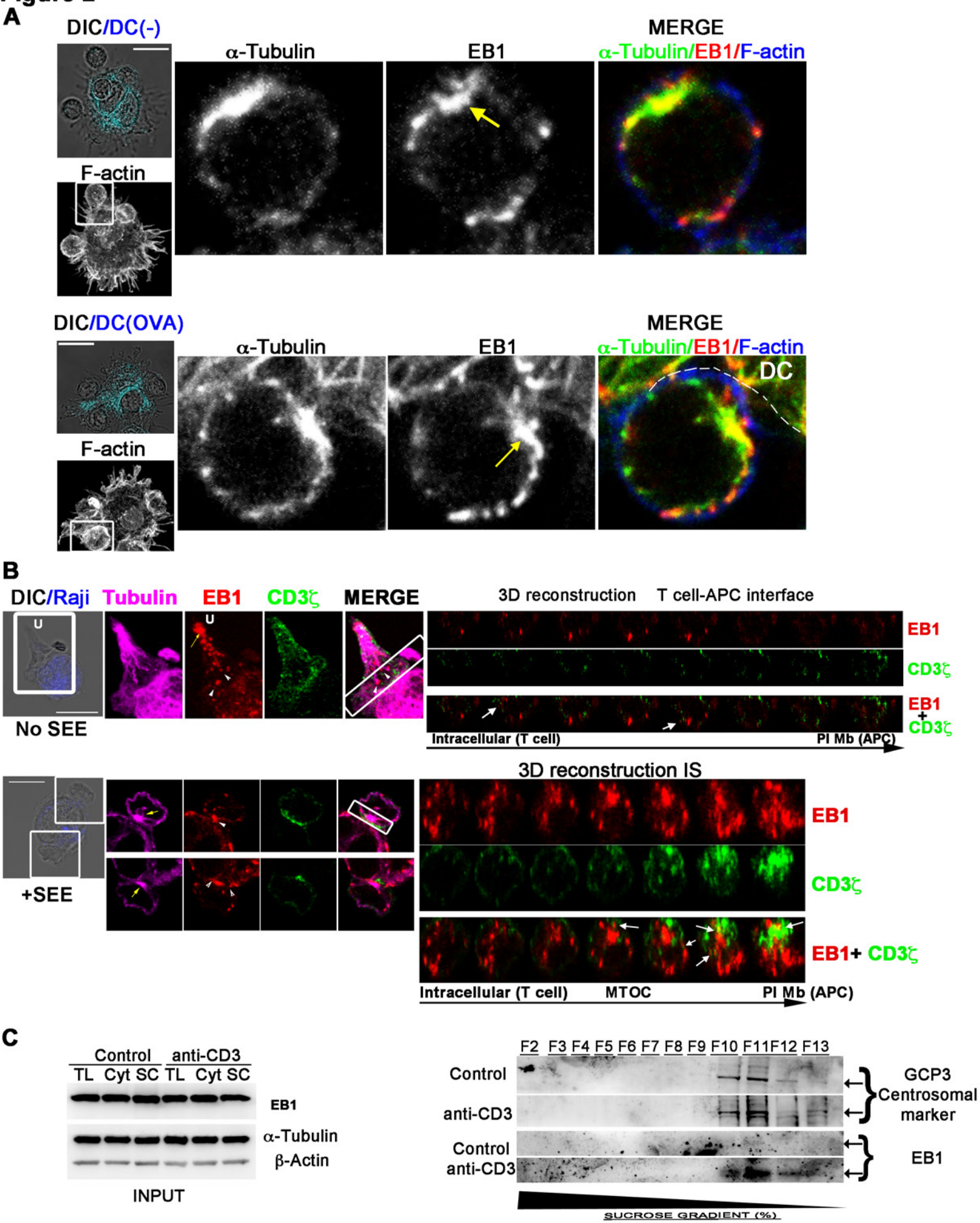
A
DIC/DC(-)
α-Tubulin
EB1
MERGE
α-Tubulin/EB1/F-actin
F-actin
DIC/DC(OVA)
α-Tubulin
EB1
MERGE
α-Tubulin/EB1/F-actin
DC
F-actin
B
DIC/Raji
Tubulin
EB1
CD3ζ
MERGE
3D reconstruction
T cell-APC interface
EB1
CD3ζ
EB1 + CD3ζ
Intracellular (T cell)
Pl Mb (APC)
No SEE
3D reconstruction IS
+SEE
EB1
CD3ζ
EB1+ CD3ζ
Intracellular (T cell)
MTOC
Pl Mb (APC)
C
Control
anti-CD3
TL Cyt SC TL Cyt SC
EB1
α-Tubulin
β-Actin
INPUT
F2 F3 F4 F5 F6 F7 F8 F9 F10 F11 F12 F13
Control
anti-CD3
GCP3
Centrosomal
marker
Control
anti-CD3
EB1
SUCROSE GRADIENT (%)

Figure 3

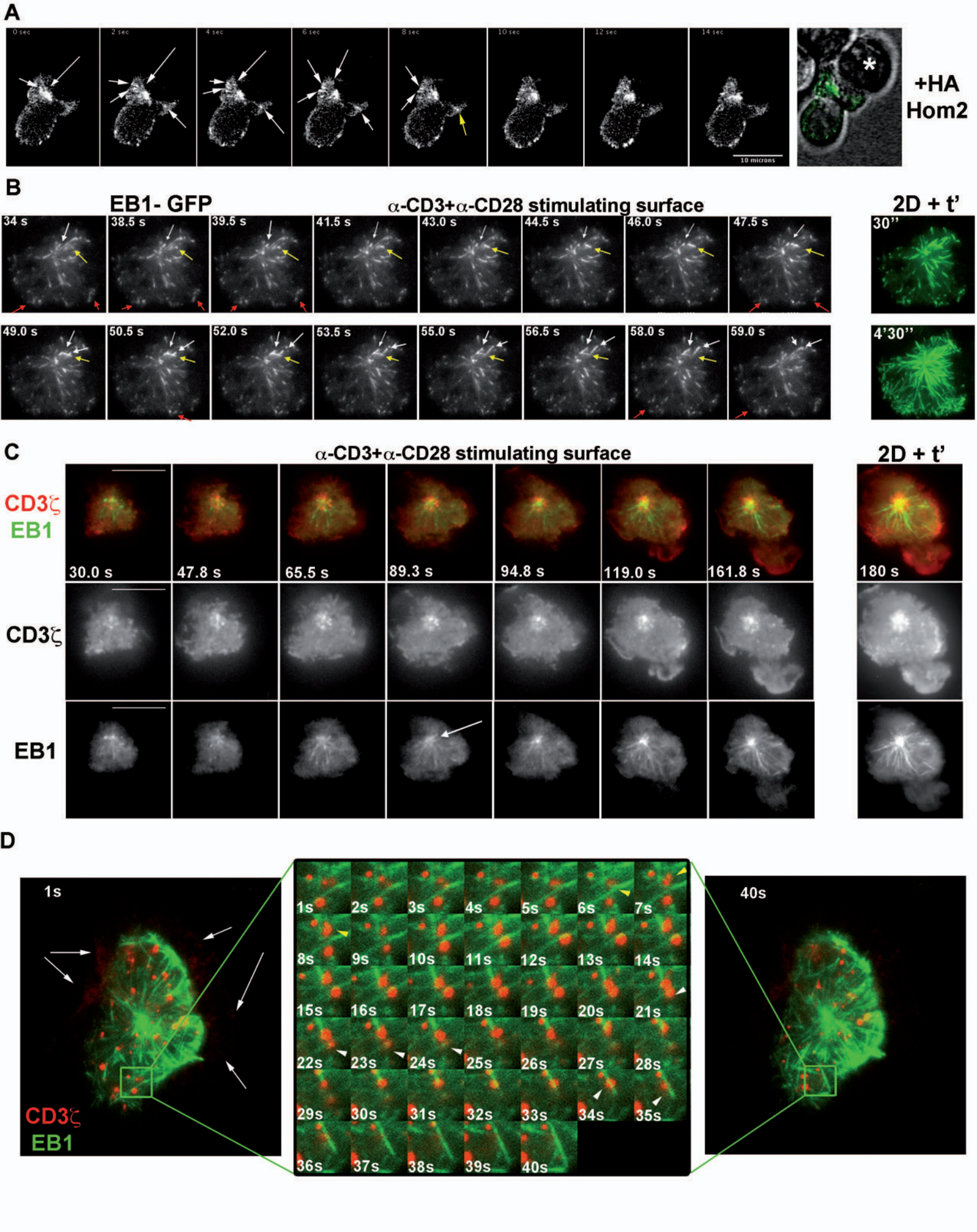
A
0 sec
2 sec
4 sec
6 sec
8 sec
10 sec
12 sec
14 sec
10 microns
+HA
Hom2
B
EB1- GFP
α-CD3+α-CD28 stimulating surface
2D + t'
34 s
38.5 s
39.5 s
41.5 s
43.0 s
44.5 s
46.0 s
47.5 s
30''
49.0 s
50.5 s
52.0 s
53.5 s
55.0 s
56.5 s
58.0 s
59.0 s
4'30''
C
α-CD3+α-CD28 stimulating surface
2D + t'
CD3ζ
EB1
30.0 s
47.8 s
65.5 s
89.3 s
94.8 s
119.0 s
161.8 s
180 s
CD3ζ
EB1
D
1s
CD3ζ
EB1
1s
2s
3s
4s
5s
6s
7s
8s
9s
10s
11s
12s
13s
14s
15s
16s
17s
18s
19s
20s
21s
22s
23s
24s
25s
26s
27s
28s
29s
30s
31s
32s
33s
34s
35s
36s
37s
38s
39s
40s
40s

Figure 4

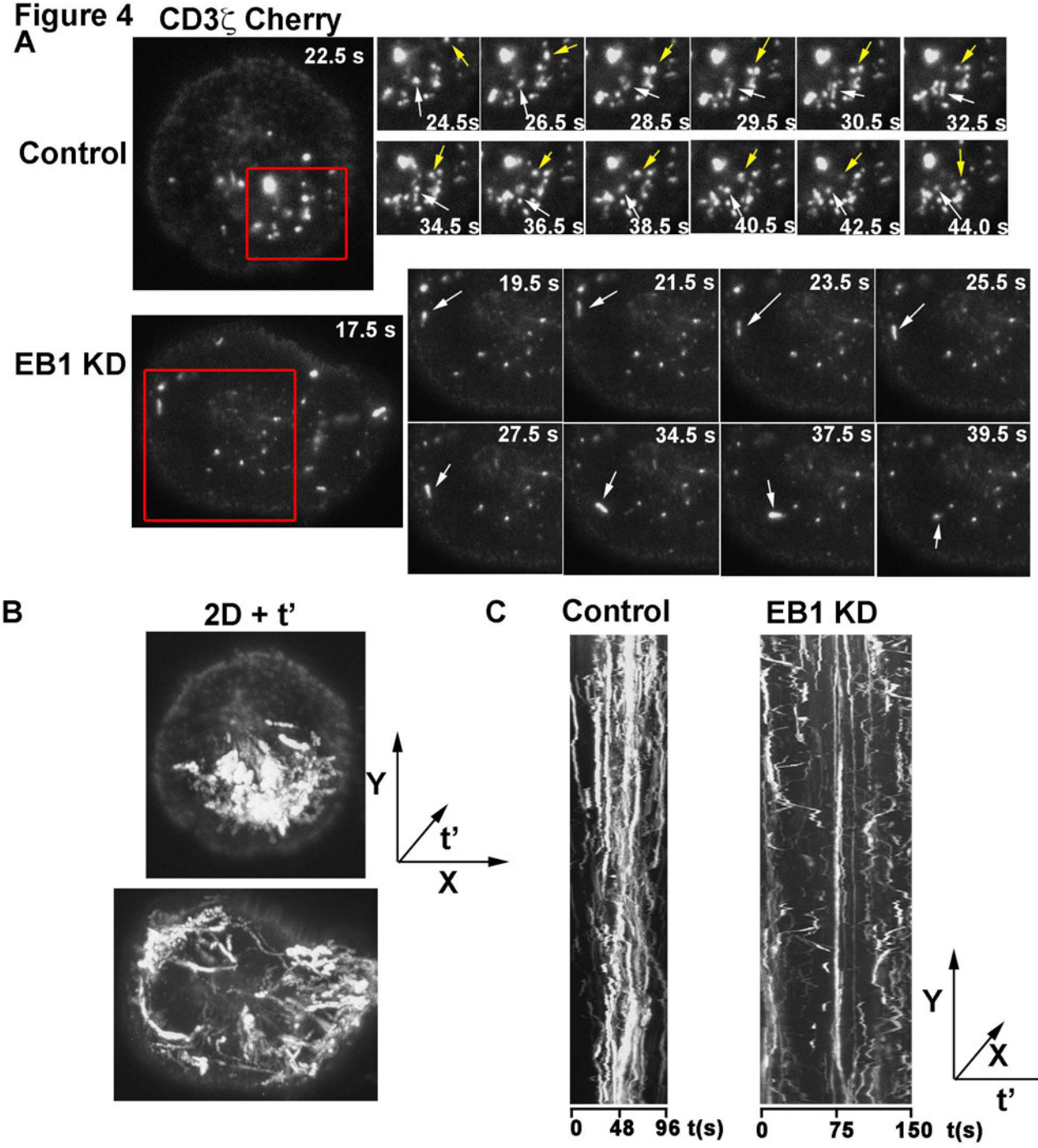
A
CD3ζ Cherry
Control
22.5 s
24.5s
26.5 s
28.5 s
29.5 s
30.5 s
32.5 s
34.5 s
36.5 s
38.5 s
40.5 s
42.5 s
44.0 s
EB1 KD
17.5 s
19.5 s
21.5 s
23.5 s
25.5 s
27.5 s
34.5 s
37.5 s
39.5 s
B
2D + t'
Y
t'
X
C
Control
EB1 KD
0 48 96 t(s)
0 75 150 t(s)
Y
X
t'
D
EB1
CD3ζ
CD3ζ/EB1
3D at the IS
DIC/Raji
Control IS plane
EB1 KD IS plane
CD3ζ at the IS
P<0.0001
CD3ζ MFI/Area (A.U./μm²)
Control
EB1 KD
EB1 at the IS
P<0.0001
EB1 MFI/Area (A.U./μm²)
Control
EB1 KD

Figure 5

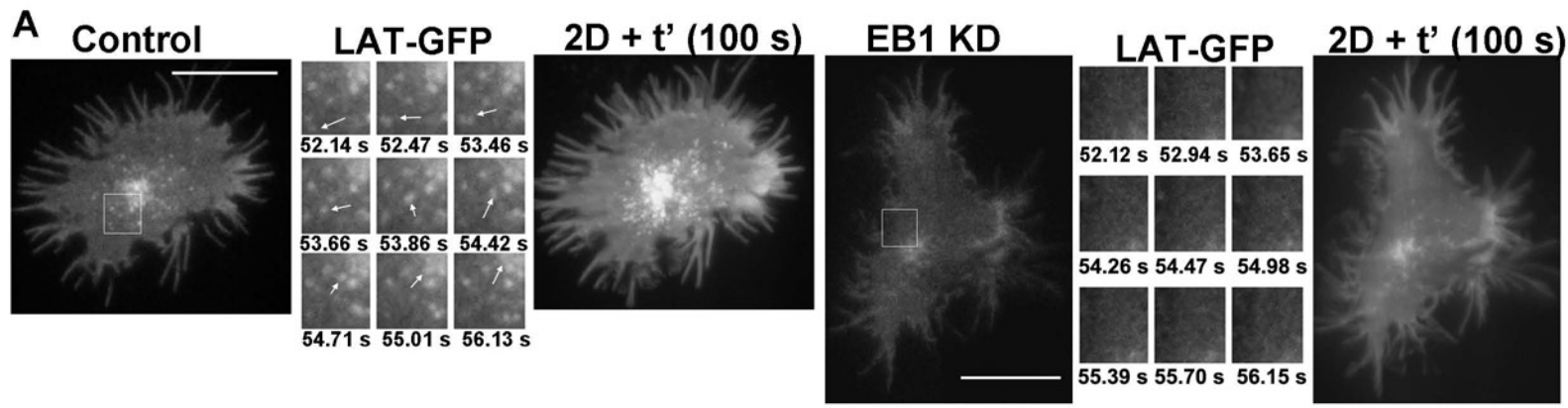
A
Control
LAT-GFP
2D + t' (100 s)
EB1 KD
LAT-GFP
2D + t' (100 s)
52.14 s
52.47 s
53.46 s
53.66 s
53.86 s
54.42 s
54.71 s
55.01 s
56.13 s
52.12 s
52.94 s
53.65 s
54.26 s
54.47 s
54.98 s
55.39 s
55.70 s
56.15 s

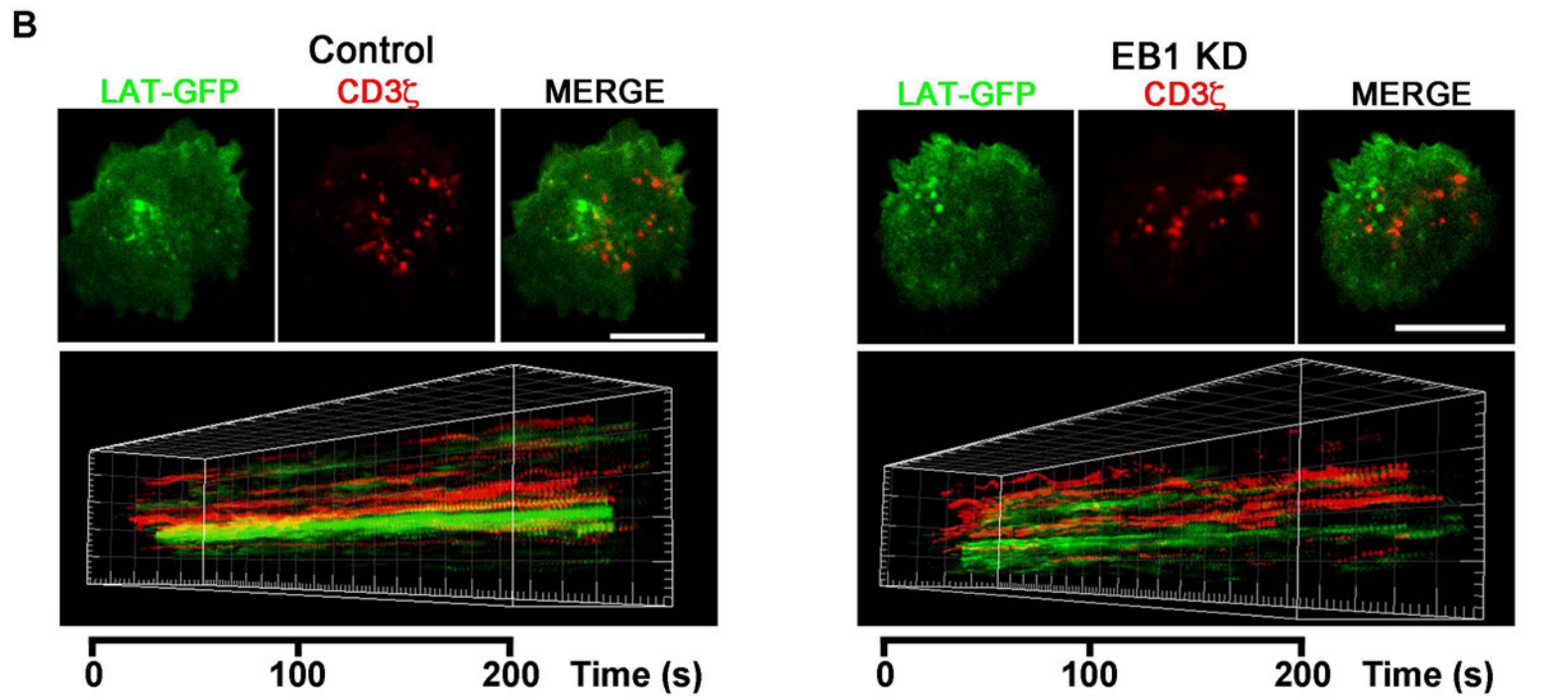
B
Control
LAT-GFP
CD3ζ
MERGE
EB1 KD
LAT-GFP
CD3ζ
MERGE
0
100
200
Time (s)
0
100
200
Time (s)

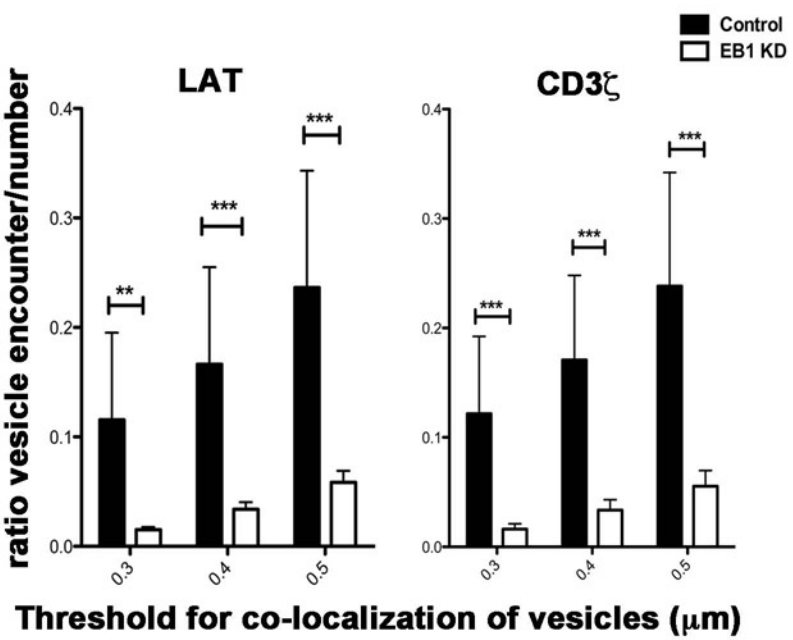
Control
EB1 KD
LAT
CD3ζ
ratio vesicle encounter/number
0.0
0.1
0.2
0.3
0.4
**
***
***
***
***
***
0.3
0.4
0.5
0.3
0.4
0.5
Threshold for co-localization of vesicles (μm)

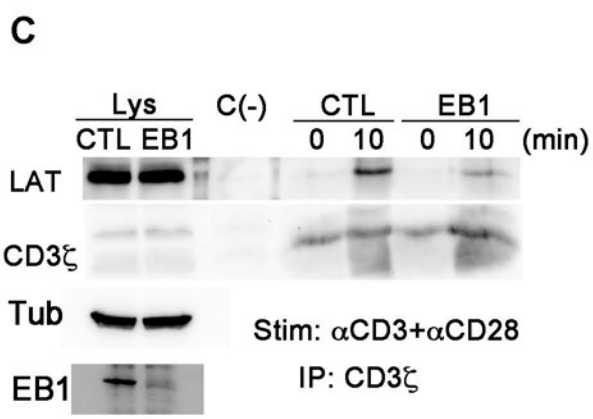
C
Lys
CTL EB1
C(-)
CTL
EB1
0 10 0 10 (min)
LAT
CD3ζ
Tub
EB1
Stim: αCD3+αCD28
IP: CD3ζ

Figure 6

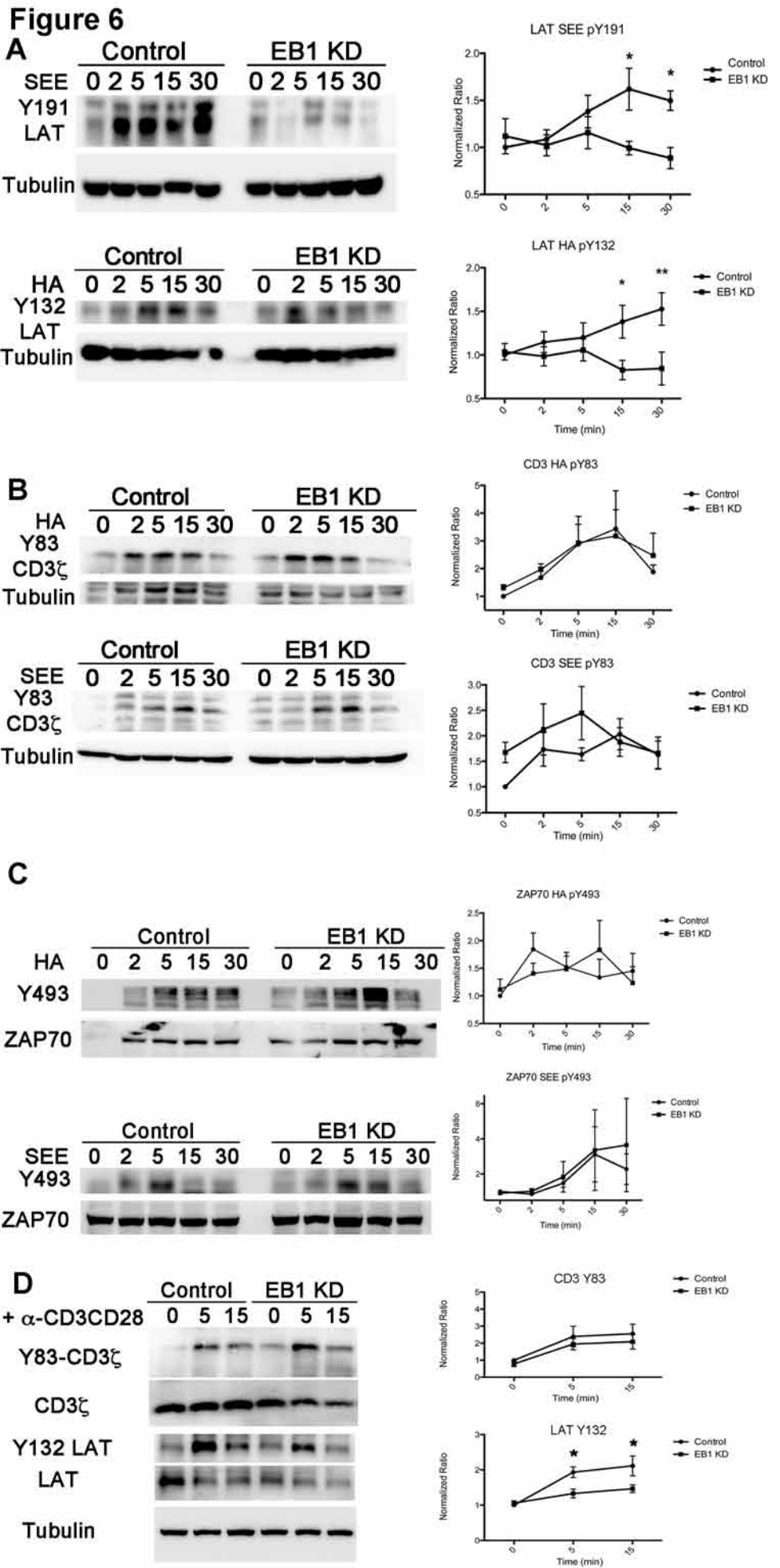
A
Control
EB1 KD
SEE
0 2 5 15 30
0 2 5 15 30
Y191
LAT
Tubulin
LAT SEE pY191
Normalized Ratio
Control
EB1 KD
HA
Y132
LAT
LAT HA pY132
Time (min)
B
CD3 HA pY83
CD3 SEE pY83
Y83
CD3ζ
C
ZAP70 HA pY493
ZAP70 SEE pY493
Y493
ZAP70
D
+ α-CD3CD28
0 5 15 0 5 15
Y83-CD3ζ
CD3ζ
Y132 LAT
CD3 Y83
LAT Y132

Figure 7

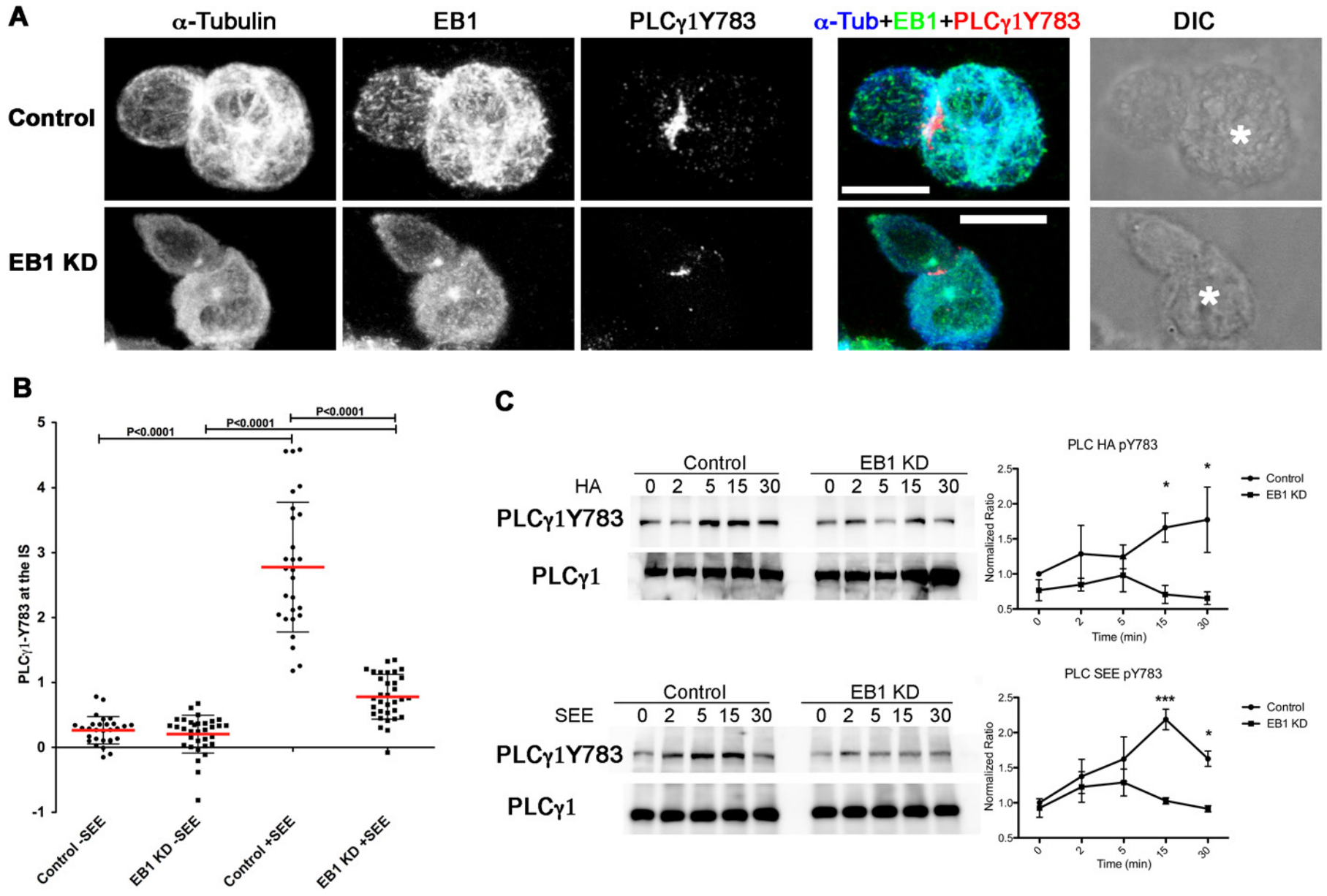
A
α-Tubulin
EB1
PLCγ1Y783
α-Tub+EB1+PLCγ1Y783
DIC
Control
EB1 KD
B
P<0.0001
P<0.0001
P<0.0001
PLCγ1-Y783 at the IS
5
4
3
2
1
0
-1
Control -SEE
EB1 KD -SEE
Control +SEE
EB1 KD +SEE
C
Control
EB1 KD
HA
0 2 5 15 30
0 2 5 15 30
PLCγ1Y783
PLCγ1
PLC HA pY783
Normalized Ratio
Time (min)
Control
EB1 KD
SEE
PLC SEE pY783
***

Supplemental Figure S1

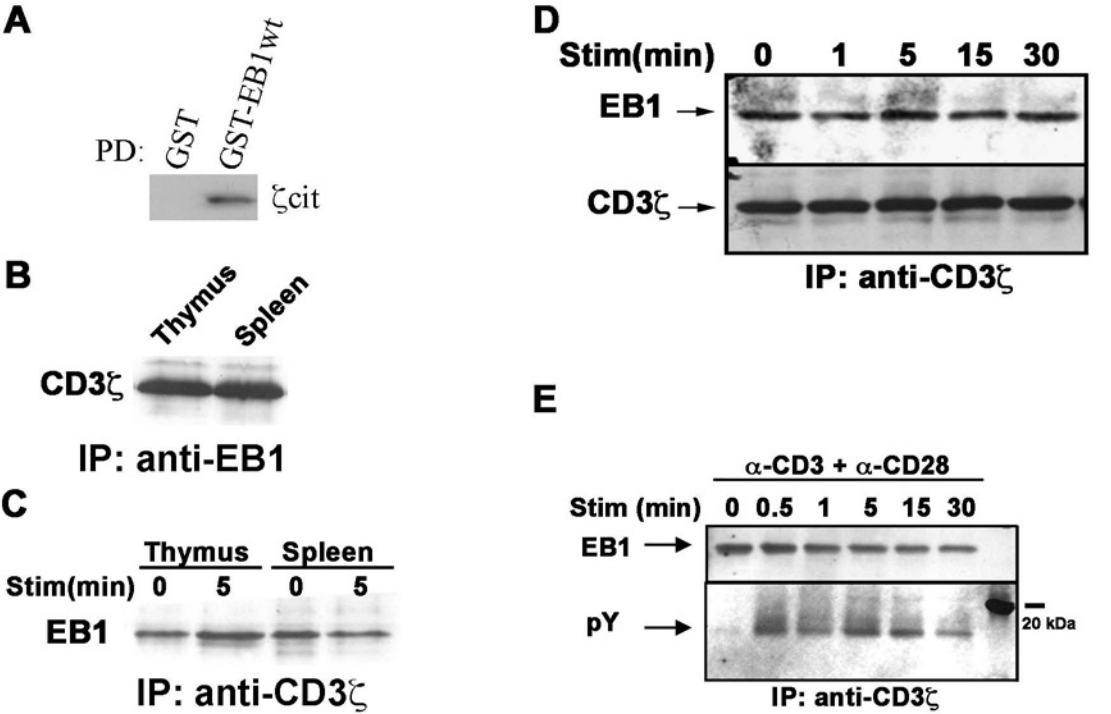

Supplemental Figure S2

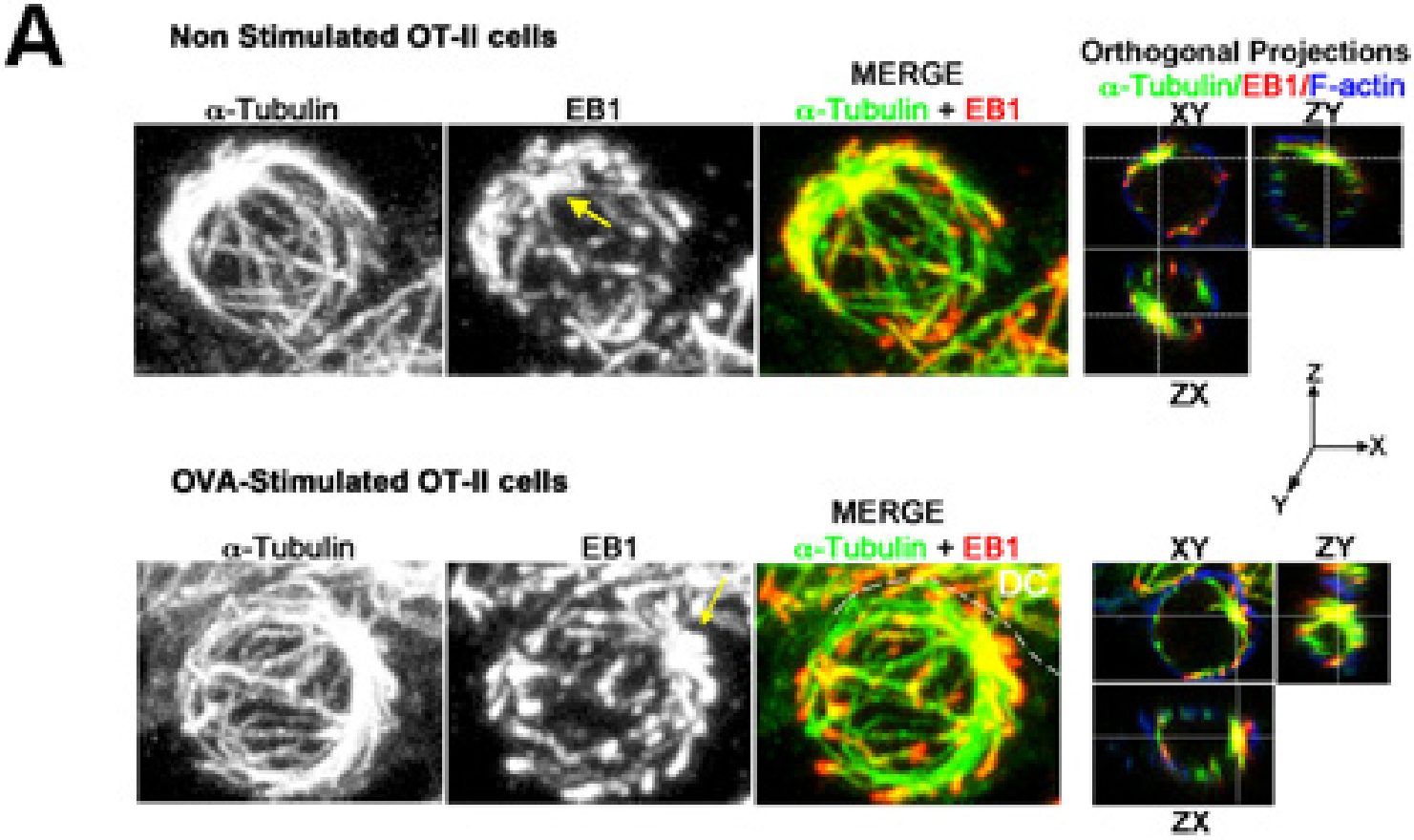

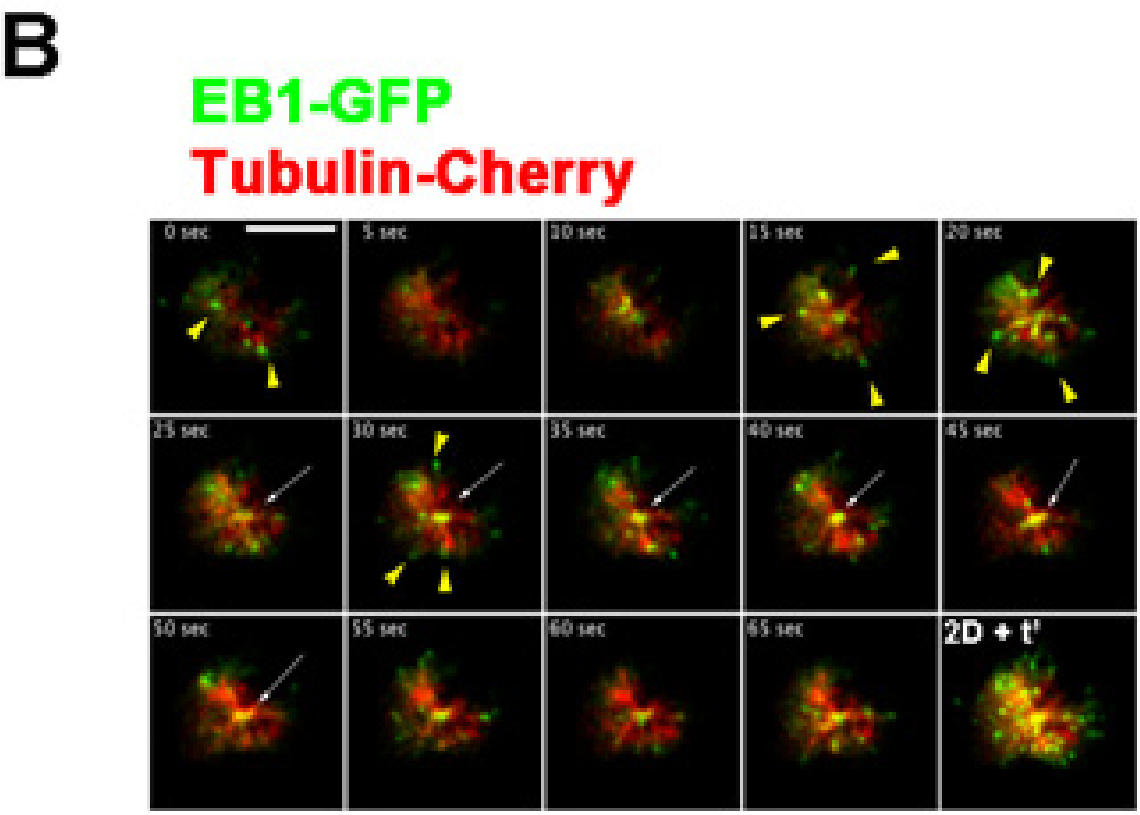

Supplemental Figure S3

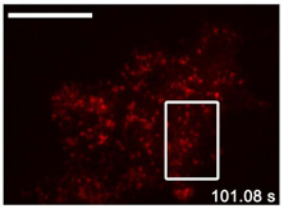

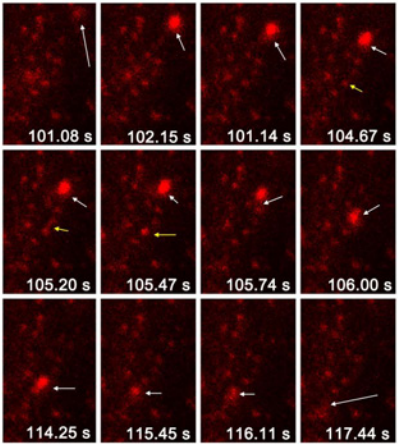

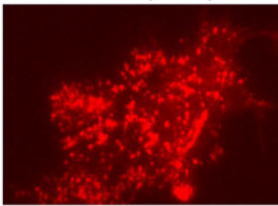

Supplemental Figure S4

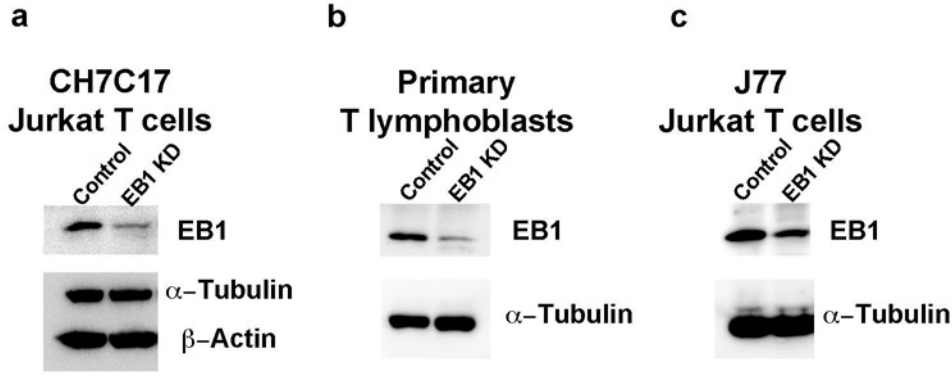

Supplemental Figure S5

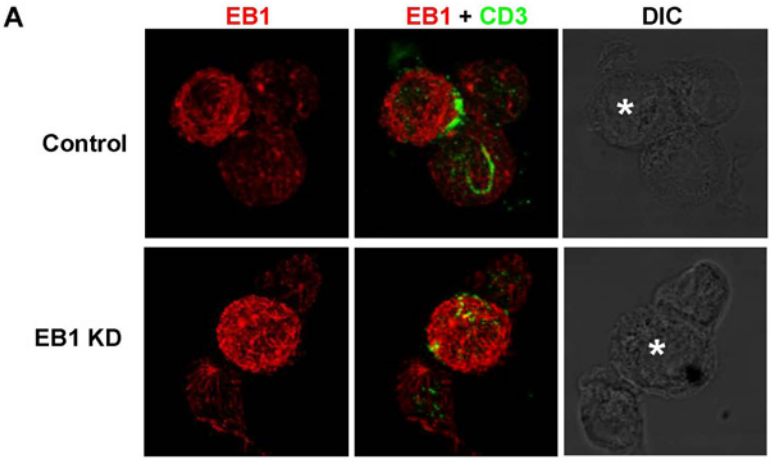

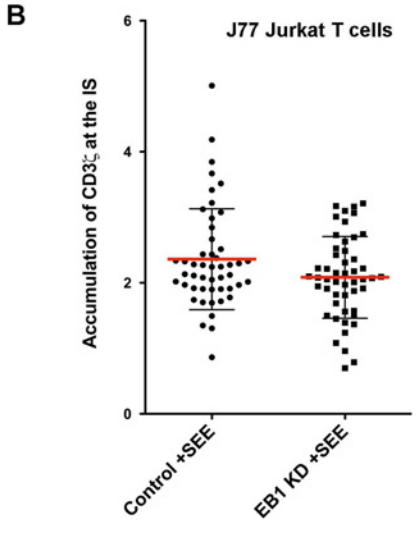

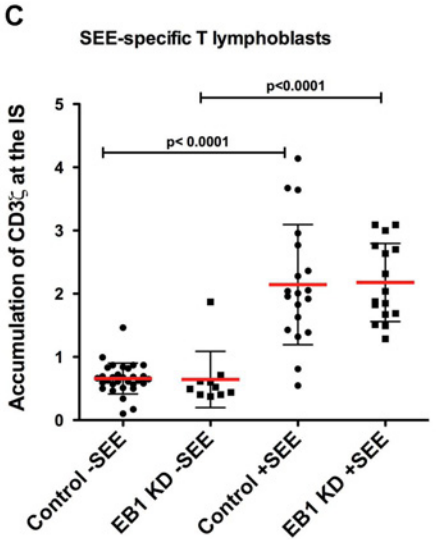

Supplemental Figure S6

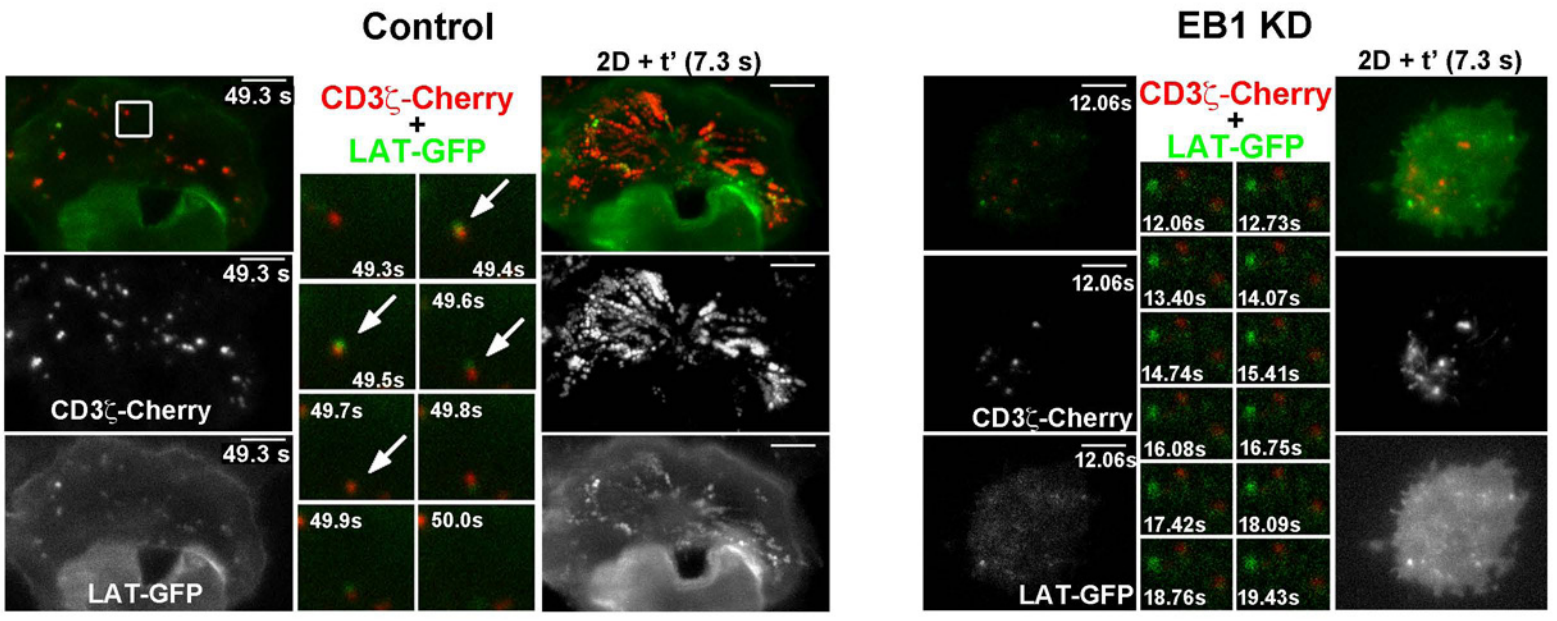

Supplemental figure S7

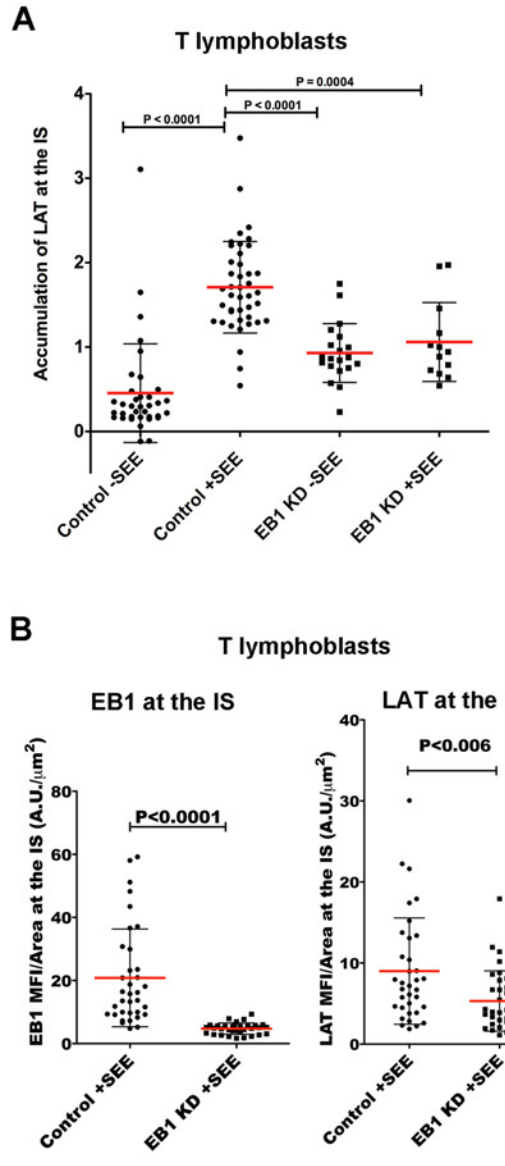

Figure 1A: GST pull-down for EB1

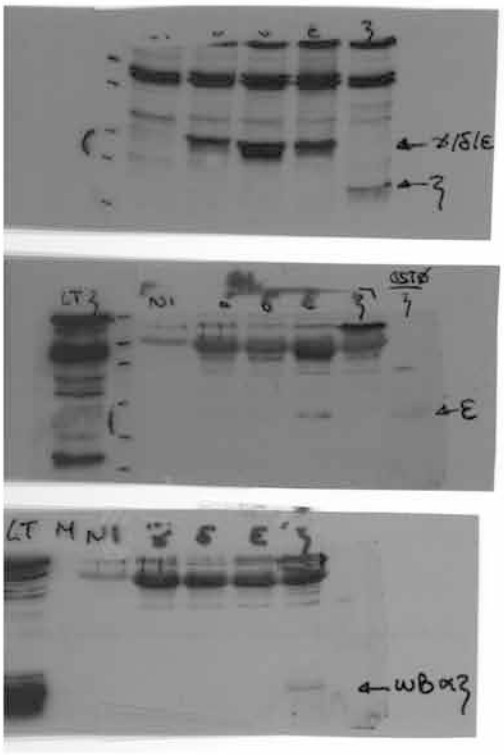

Figure 1B: IP for HA-EB1

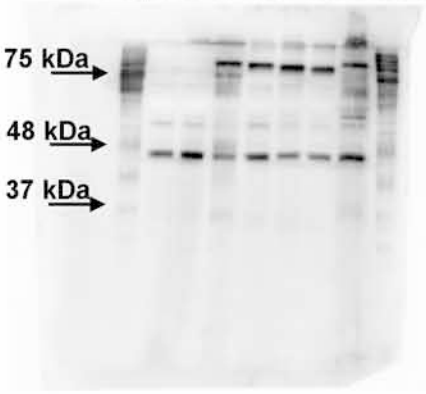

Total lysates WB: CD8

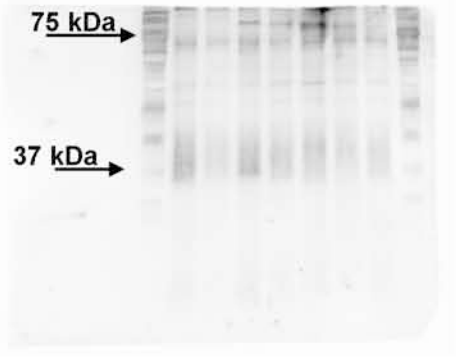

IP: HA WB: CD8
Non-reducing

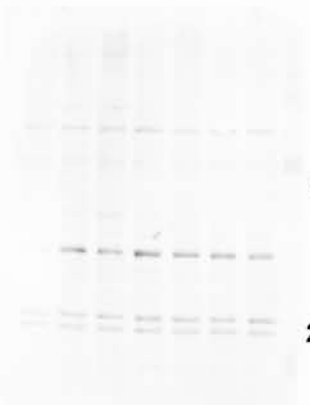

Total lysates WB: HA

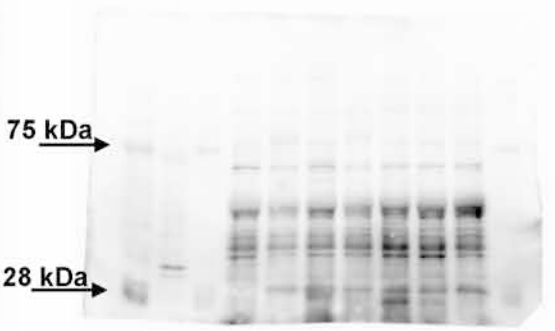

IP: HA WB: HA

Figure 1C: Pull-down

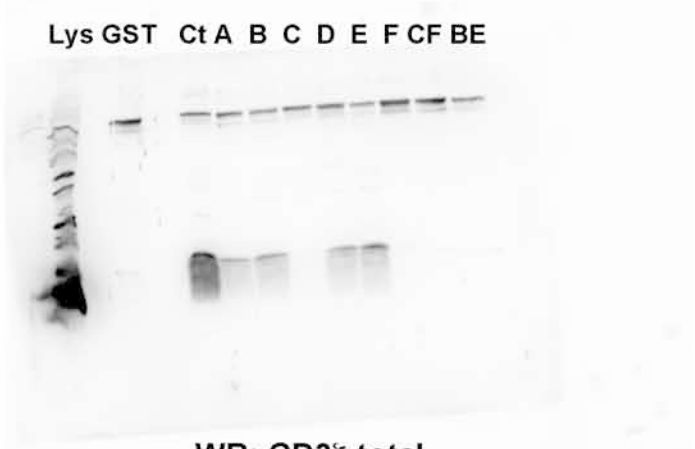

WB: CD3ζ total

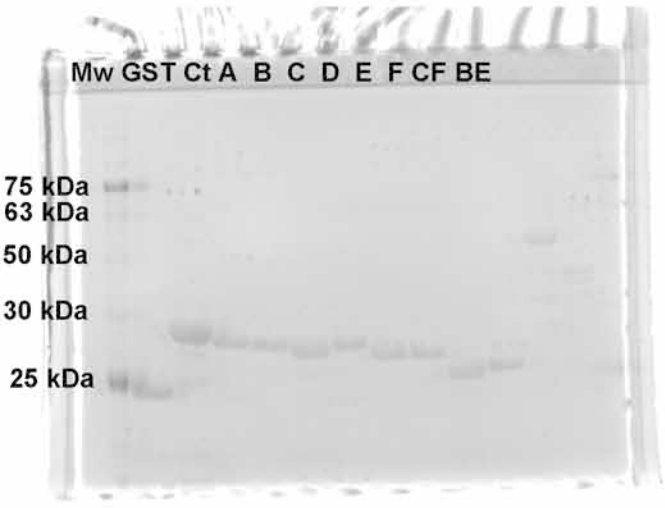

GST loading Coomassie

Figure 1D: IP with different antibodies.
Biotinylated cell surface proteins

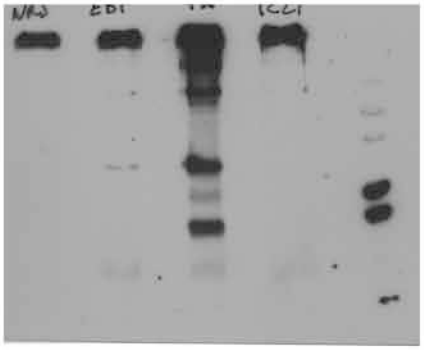

30 sec

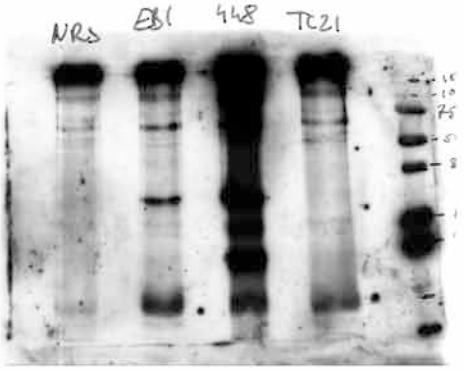

30 min

WB: streptavidin-HRP

Figure 1E: IP with anti-EB1. APC: antigen-presenting cells. Ratio T.APC, 1:10

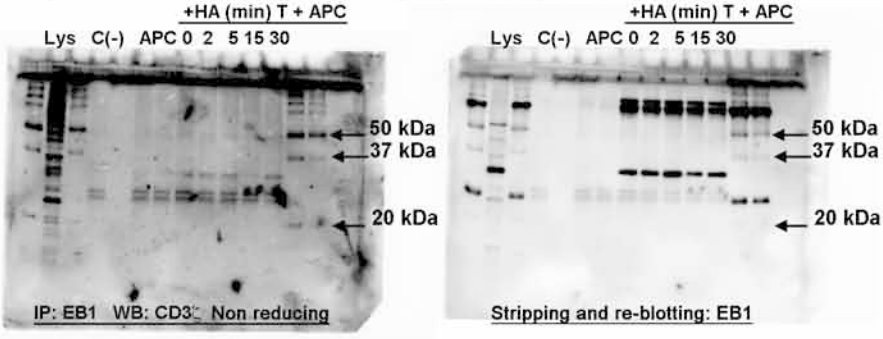

Figure 2C

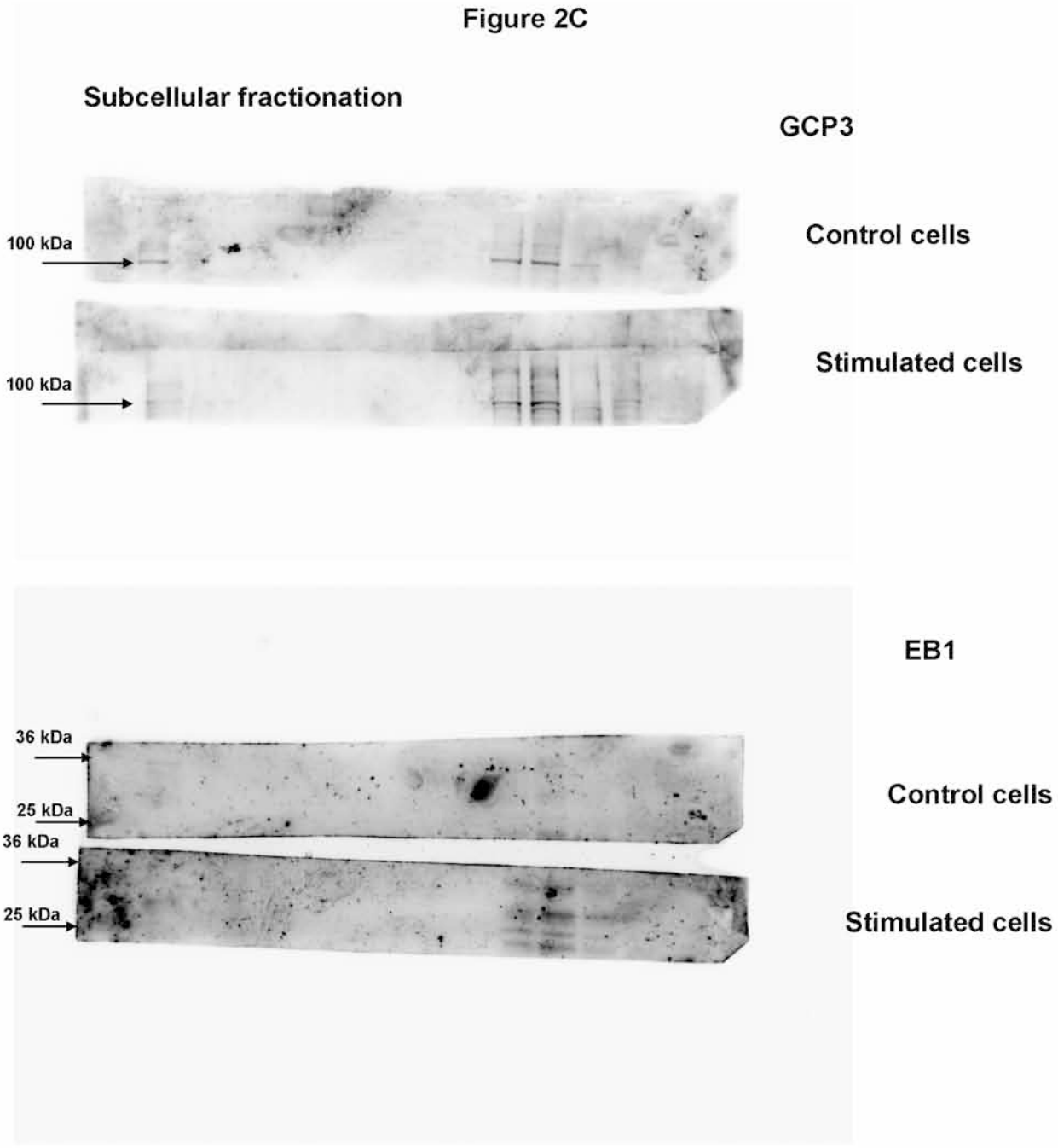
Subcellular fractionation
GCP3
100 kDa
Control cells
100 kDa
Stimulated cells
EB1
36 kDa
25 kDa
Control cells
36 kDa
25 kDa
Stimulated cells
Lysates previous to the fractionation
37 kDa
EB1
50 kDa
Tubulin
Actin

Figure 5C: IP for CD3ζ in control and EB1-silenced T cells.

WB: Tubulin

WB: EB1

IP: CD3ζ WB: CD3ζ

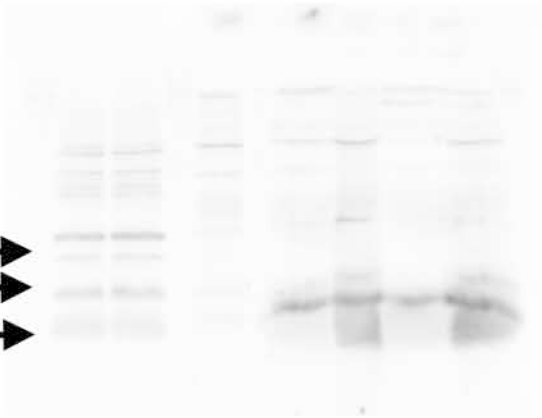

IP: Non reducing; Iodoacetamide-treated samples

WB: 2-mercaptoethanol-treated samples

IP: CD3ζ WB: LAT

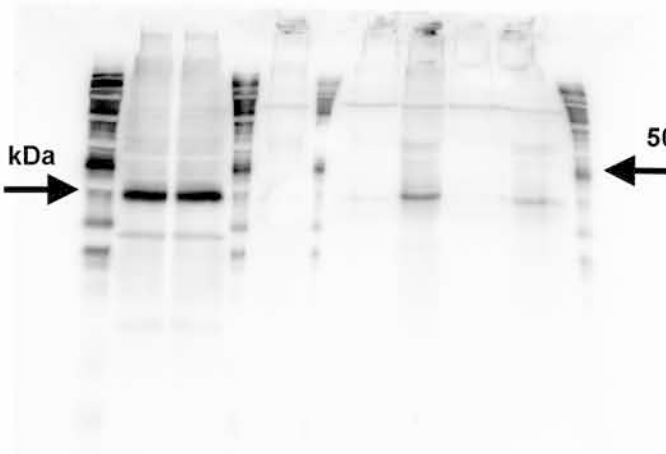

Figure 6

LAT Y132

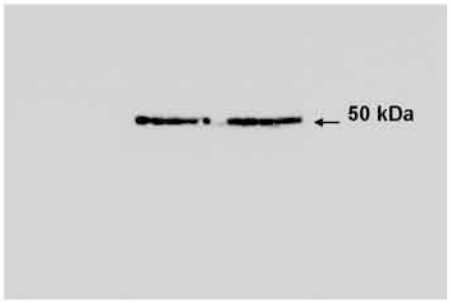

Tubulin

Figure 6A
HA stimulation

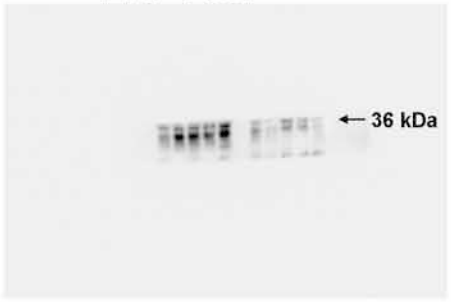

LAT Y191

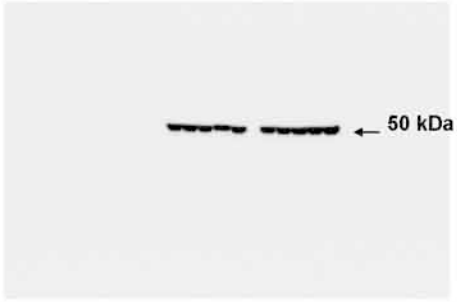

Tubulin

Figure 6A
SEE stimulation

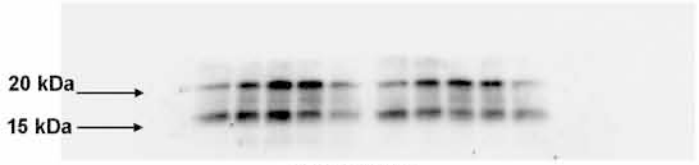

CD3 Y83

Tubulin

Figure 6B
HA stimulation

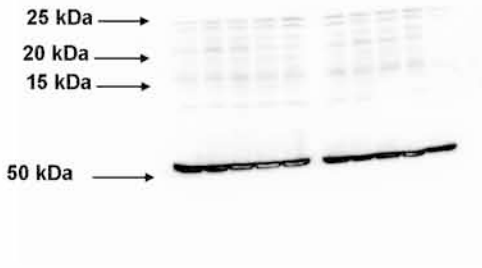

CD3 Y83

Tubulin

Figure 6B
SEE stimulation

ZAP70 Y493

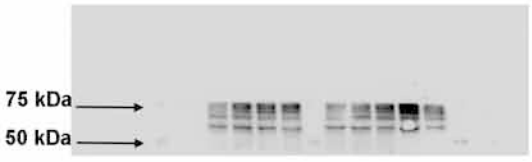

ZAP70 total

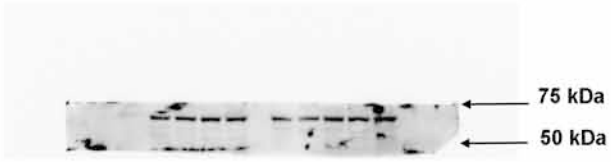

Figure 6C
HA stimulation

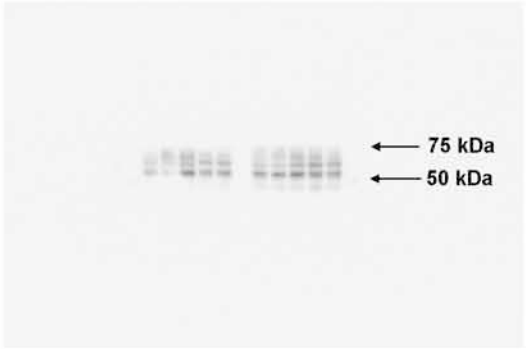

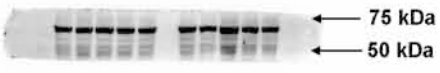

Figure 6C
SEE stimulation

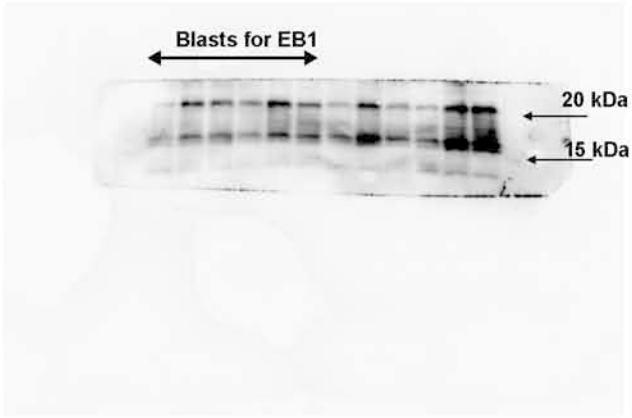

CD3ζ Y83

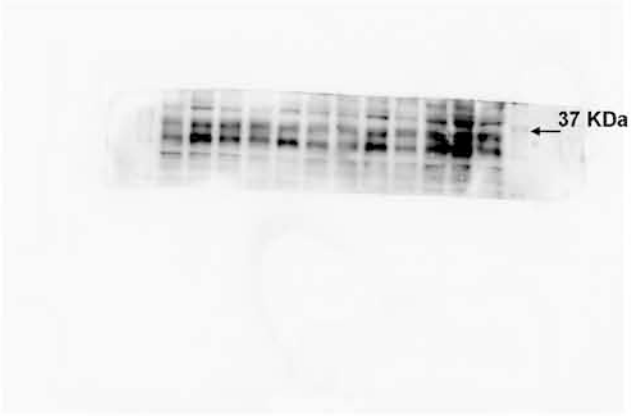

LAT Y132

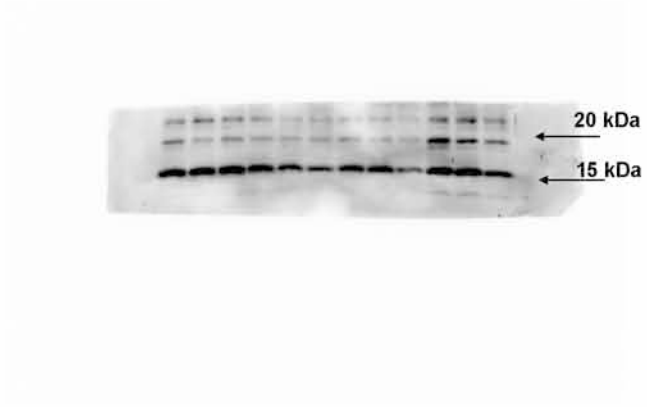

CD3ζ total

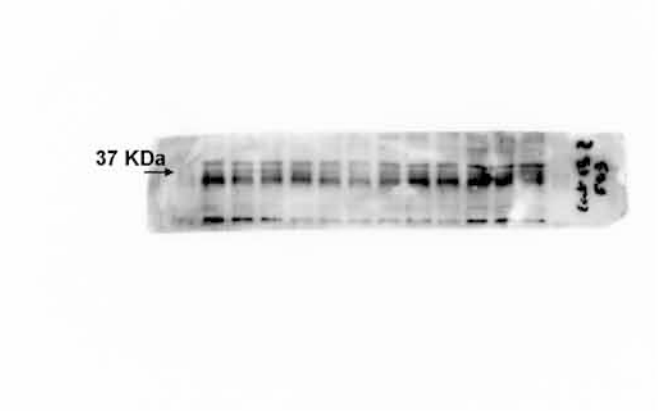

LAT total

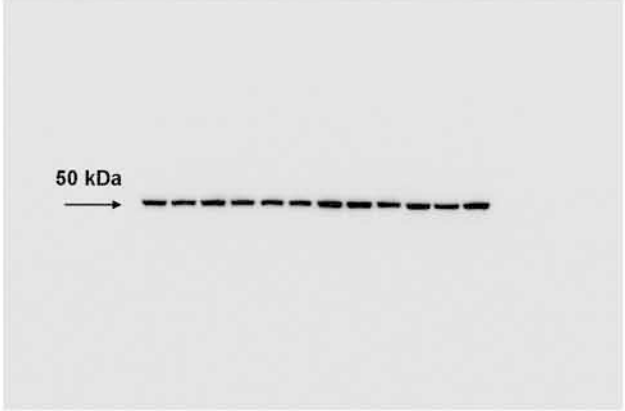

Tubulin

Figure 7C

HA-stimulated CH7C17 T cells

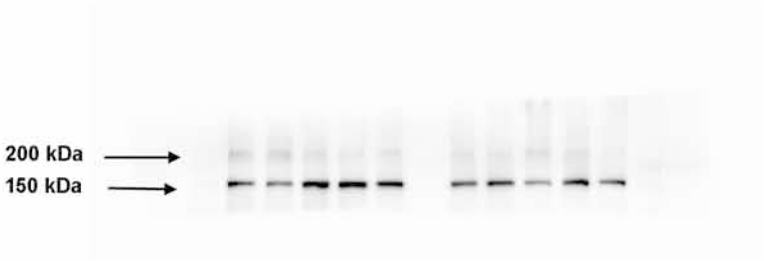

PLC Y783

PLC total

SEE-stimulated T lymphoblasts

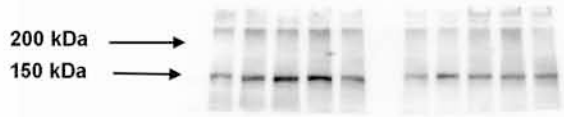

PLC Y783

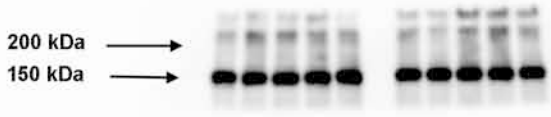

PLC total